HHS Public Access

Author manuscript

Neuroscience. Author manuscript; available in PMC 2016 September 10.

Published in final edited form as:

Neuroscience. 2015 September 10; 303: 604–629. doi:10.1016/j.neuroscience.2015.07.026.

Connexin36 expression in major centers of the auditory system in the CNS of mouse and rat: Evidence for neurons forming purely electrical synapses and morphologically mixed synapses

M.E. Rubio[a] and **J.I. Nagy**[b]

[a]Departments of Otolaryngology and Neurobiology, University of Pittsburgh Medical School, Pittsburgh, USA

[b]Department of Physiology and Pathophysiology, Faculty of Medicine, University of Manitoba, Winnipeg, Canada

Abstract

Electrical synapses formed by gap junctions composed of connexin36 (Cx36) are widely distributed in the mammalian central nervous system (CNS). Here, we used immunofluorescence methods to document the expression of Cx36 in the cochlear nucleus and in various structures of the auditory pathway of rat and mouse. Labelling of Cx36 visualized exclusively as Cx36-puncta was densely distributed primarily on the somata and initial dendrites of neuronal populations in the ventral cochlear nucleus, and was abundant in superficial layers of the dorsal cochlear nucleus. Other auditory centers displaying Cx36-puncta included the medial nucleus of the trapezoid body (MNTB), regions surrounding the lateral superior olivary nucleus, the dorsal nucleus of the medial lemniscus, the nucleus sagulum, all subnuclei of the inferior colliculus, and the auditory cerebral cortex. In EGFP-Cx36 transgenic mice, EGFP reporter was detected in neurons located in each of auditory centers that harboured Cx36-puncta. In the ventral cochlear nuclei and the MNTB, many neuronal somata were heavily innervated by nerve terminals containing vesicular glutamate transporter-1 (vglut1) and Cx36 was frequently localized at these terminals. Cochlear ablation caused a near total depletion of vglut1-positive terminals in the ventral cochlear nuclei, with a commensurate loss of labelling for Cx36 around most neuronal somata, but preserved Cx36-puncta at somatic neuronal appositions. The results suggest that electrical synapses formed by Cx36-containing gap junctions occur in most of the widely distributed centers of the auditory system. Further, it appears that morphologically mixed chemical/electrical synapses formed by nerve terminals are abundant in the ventral cochlear nucleus, including those at endbulbs of Held

Address for correspondence Dr. James I. Nagy Department of Physiology Faculty of Medicine University of Manitoba 745 Bannatyne Ave, Winnipeg, Manitoba Canada R3E 0J9 nagyji@ms.umanitoba.ca Tel. (204) 789-3767 Fax (204) 789-3934.

Neuroimage data

Neuroimage 1. Movie file of the image in Fig. 8A (z-stack of 5.2 μm), showing labelling for Cx36 (red) and vglut1 (green), showing association of Cx36 puncta with vglut1-positive nerve terminals (green) in the AVCN, with various angles of rotation.

Neuroimage 2. Labelling of Cx36 (red) and vglut1 (green) associated with an octopus cell in the PVCN.

formed by cochlear primary afferent fibers, and those at calyx of Held synapses on MNTB neurons.

Keywords

Cochlear nucleus; electrical synapses; neuronal gap junctions; vesicular glutamate transporter-1; connexin36; mixed chemical/electrical synapses; calyx of Held; endbulbs of Held

INTRODUCTION

Gap junctions at cell appositions are composed of connexin proteins that form intercellular channels allowing cell-to-cell passage of ions and small molecules (Goodenough and Paul, 2009; Herve and Derangeon, 2013). In neural systems, gap junctions between neurons create the structural substrate of electrical synaptic transmission (Bennett, 1997). The prevalence and physiological importance of electrical synapses between neurons in the CNS of lower vertebrates has long been recognized (Sotelo and Korn, 1978; Bennett and Goodenough, 1978). In contrast, it is only in the past decade that there has been general acceptance of the widespread occurrence and functional relevance of electrical synapses in neural circuitry of mammalian brain and spinal cord (Connors, 2009; Pereda et al., 2013; Pereda, 2014). The principle connexin component of neuronal gap junctions in mammalian systems is connexin36 (Cx36), which has been documented to occur in ultrastructurally-identified gap junctions between neurons (Rash et al., 2000, 2001), and which supports electrical synaptic transmission in many regions of the CNS (Bennett and Zukin, 2004; Connors and Long, 2004; Hormuzdi et al., 2004; Sohl et al., 2005; Meier and Dermietzel; 2006 Bautista et al., 2012). Immunohistochemical visualization of Cx36 in gap junctions at the ultrastructural level is well-correlated with its localization by immunofluorescence, at least *in vivo* (Rash et al., 2004, 2005, 2007a,b), a fortuitous feature arising from what appears to be immunolabelling and detection of Cx36 exclusively at gap junctions, with its other potential subcellular and intracellular sites apparently remaining masked and undetectable with currently available anti-Cx36 antibodies (Nagy, 2012; Nagy et al., 2013; Bautista and Nagy, 2014; Bautista et al., 2014). Thus, Cx36 represents at least one marker for allowing light microscopic immunofluorescence identification of Cx36-containing neuronal gap junctions and reveals their cellular localization. Notwithstanding current evidence for widely distributed networks of electrically coupled neurons, our ongoing surveys of Cx36 in the entire CNS of mice and rats continues to reveal numerous additional structures that display remarkable patterns of immunolabelling for Cx36 (Nagy, unpublished observations). These include brain regions that have not been previously explored for the existence of neuronal gap junctions, or those where evidence for electrical synapses has been reported, but which have not yet been examined by immunofluorescence labelling of Cx36 with the utility of this connexin providing a broadly defining marker of neuronal gap junctions. These structures are best exemplified by various nuclei in the auditory system, which are the focus of the present study.

The cochlear nuclei were among the first areas found to harbour neuronal gap junctions in the mammalian CNS. Within subdivisions of this structure, somato-somatic, somato-

dendritic and dendro-dendritic gap junctions at what we refer to here as “purely electrical synapses” were reported to occur in the anteroventral cochlear nucleus (AVCN) as well as the dorsal cochlear nucleus (DCN) (Sotelo, 1975; Sotelo et al., 1976; Wouterlood et al., 1984; Mugnaini, 1985). In addition, another type of electrical synapse formed by gap junctions between an axon terminal and a postsynaptic neuron, which was found to have wide occurrence in lower vertebrates (Bennett and Goodenough, 1978) and termed “mixed synapses” with potential for dual chemical and electrical transmission, has been described in the ventral cochlear nucleus (Sotelo and Triller, 1982). Subsequent to these early reports, molecular and/or morphological correlates of electrical synapses, and electrical coupling via these synapses between cochlear neurons, has been the subject of only a few reports. As in most CNS regions found to contain neuronal gap junctions composed of Cx36, it has been noted that cochlear neurons express moderate levels of Cx36 mRNA (Condorelli et al., 2000). However, Cx36 protein was not detected in the cochlear nucleus of mouse, but was reported to occur in this nucleus of brown bats (Howowitz et al., 2008). More recently, ultrastructural studies have described neuronal gap junctions between the somata of bushy cells in the AVCN of rat and monkey (Gómez-Nieto and Rubio, 2009, 2011). In addition, *in vitro* electrophysiological approaches have demonstrated functional electrical coupling between stellate cells and fusiform cells in the dorsal cochlear nucleus (DCN) (Apostolides and Trussell, 2013).

Here, we examined Cx36 expression by immunofluorescence localization of this connexin in various subdivisions of the cochlear nucleus and other nuclei in the ascending auditory system in the CNS of mouse and rat. We used Cx36 knockout mice to confirm specificity of Cx36 detection, enhanced green fluorescent protein (EGFP)-Cx36 mice to correlate Cx36-promoter driven EGFP expression with cellular distribution of Cx36, and cochlear ablation to establish primary afferent origin of the majority of immunolabelling for Cx36 in the ventral cochlear nuclei. A high level of Cx36 protein expression was found in association with neurons in each of the cochlear subnuclei, with distinct subcellular localization either at purely electrical synapses or at what appear to be morphologically mixed synapses in the ventral cochlear nuclei and in the MNTB, where Cx36 was co-localized with nerve terminals containing vesicular glutamate transporter-1 (vglut1). These results, together with moderately distributed immunolabelling of Cx36 observed in regions surrounding the lateral superior olivary nucleus, as well as within the dorsal nucleus of the medial lemniscus, all subnuclei of the inferior collicular, and in the auditory cerebral cortex, suggest that electrical synapses are a consistent feature in most divisions of the central auditory system.

EXPERIMENTAL PROCEDURES

Animals and antibodies

A total of twenty-two adult (>2 months of age) male Sprague-Dawley rats, twenty adult male C57 BL/6-129SvEv mice and three CD1 adult male mice between two and three months of age were used in this study. Animals were obtained from the Central Animal Care Services at the University of Manitoba and utilized according to approved protocols by the Central Animal Care Committee of University of Manitoba, with minimization of the numbers of animals used. The C57 BL/6-129SvEv mice used included nine wild-type and

three transgenic Cx36 knockout animals, colonies of which were established at the University of Manitoba through generous provision of wild-type and Cx36 knockout breeding pairs (Deans et al., 2001) from Dr. David Paul (Harvard). Eight transgenic adult male C57 BL/6-129SvEv mice included those in which Cx36 expression is normal and bacterial artificial chromosome provides EGFP expression driven by the Cx36 promoter, designated EGFP-Cx36 mice. These mice were taken from a colony established at the University of Manitoba starting with breeding pairs obtained from UC Davis Mutant Mouse Regional Resource Center (Davis, CA, USA; see also http://www.gensat.org/index.html). Data from mice and rats were compared for correspondence of results, and the mice further served to confirm antibody specificity of Cx36 detection by comparison of immunolabelling in wild-type *vs.* Cx36 knockout animals.

Two polyclonal antibodies (Cat. No. 36-4600 and Cat. No. 51-6300) and one monoclonal antibody (Cat. No. 39-4200) against Cx36 were obtained from Life Technologies Corporation (Grand Island, NY, USA) (formerly Invitrogen/Zymed Laboratories), and have been previously characterized for specificity of Cx36 detection in various regions of rodent brain (Li et al., 2004; Rash et al., 2007a,b; Curti et al., 2012). These antibodies were used at a concentration of 1-2 μg/ml in primary antibody incubations with tissue sections. Other antibodies included a guinea pig polyclonal anti-vglut1 and a guinea pig polyclonal anti-vglut2 obtained from Millipore (Temecula, CA, USA) and both were used at a dilution of 1:1000, a anti-calbindin D28K antibody obtained from Sigma Aldridge (Oakvile, Ontario, Canada) and used at a dilution of 1:000, and a rabbit monoclonal anti-EGFP (Life Technologies; Cat. No. G10362) used at a concentration of 1-2 μg/ml to immunollabel EGFP in sections from EGFP-Cx36 mice. Secondary antibodies included Cy3-conjugated goat or donkey anti-mouse IgG diluted 1:600 (Jackson ImmunoResearch Laboratories, West Grove, PA, USA), Alexa Flour 488-conjugated goat or donkey anti-rabbit and anti-mouse IgG diluted 1:600 (Molecular Probes, Eugene, OR, USA), and Cy5-conjugated goat anti-mouse IgG diluted 1:500 (Jackson ImmunoResearch Laboratories). All antibodies were diluted in 50 mM Tris-HCl, pH 7.4, containing 1.5% sodium chloride (TBS) and 0.3% Triton X-100 (TBSTr) containing 10% normal goat or normal donkey serum.

Light microscope immunofluorescence

Animals were deeply anesthetised with equithesin (3 ml/kg), placed on a bed of ice, and transcardially perfused with 0.1-0.2 ml per gram body weight of cold (4°C) pre-fixative consisting of 50 mM sodium phosphate buffer, pH 7.4, 0.1% sodium nitrite, 0.9% NaCl and 1 unit/ml of heparin. For immunolabelling of Cx36 and vglut1, animals were then perfused with 0.5 to 1 ml per gram body weight of fixative solution containing cold 0.16 M sodium phosphate buffer, pH 7.4, 0.2% picric acid and either 1% or 2% formaldehyde diluted from a 20% stock solution (Electron Microscopy Sciences, Hatfield, PA, USA). Animals were then perfused with 0.1-0.2 ml per gram body weight of a cold solution containing 10% sucrose and 25 mM sodium phosphate buffer, pH 7.4, to wash out excess fixative. Brains were removed and stored at 4°C for 24-48 h in cryoprotectant containing 25 mM sodium phosphate buffer, pH 7.4, 10% sucrose and 0.04% sodium azide. Due to the weak tissue fixation conditions used, brains were taken for sectioning no longer than a few days after cryoprotection. Transverse sections of brainstem were cut at a thickness of 10-15 μm using a

cryostat and collected on gelatinized glass slides. Slide-mounted sections could be routinely stored at −35 °C for several months before use. Considerations regarding the differential sensitivity of Cx36 *vs.* EGFP to tissue fixation and consequent difficulties in immunohistochemical detection of these proteins in combination using double labelling procedures with current commercially available antibodies have been previously discussed (Nagy et al., 2013, 2014; Bautista and Nagy, 2014). Thus, for immunolabelling of EGFP in EGFP-Cx36 mice, animals were transcardially perfused as above, except with fixative containing 4% formaldehyde, where labelling for Cx36 was substantially diminished and often abolished.

Slide mounted sections were removed from storage, air dried under a fan for 10 min, and then washed for 20 min in TBSTr. Sections processed for immunofluorescence staining as previously described (Li et al., 2008; Bautista et al., 2012; Curti et al., 2012) were incubated simultaneously with two primary antibodies for 24 h at 4°C, then washed for 1 h in TBSTr and incubated with appropriate secondary antibodies for 1.5 h at room temperature. Some sections processed for immunolabelling were counterstained with Blue Nissl NeuroTrace (stain N21479) (Molecular Probes, Eugene, OR, USA). All sections were coverslipped with the antifade medium Fluoromount-G (SouthernBiotech, Birmingham, AB, USA). Control procedures, involving omission of one of the primary antibodies with inclusion of the secondary antibodies used for double labelling, indicated absence of inappropriate cross-reactions between primary and secondary antibodies for all of the combinations used in this study.

Immunofluorescence was examined on a Zeiss Axioskop2 fluorescence microscope with Axiovision 3.0 software, a Zeiss Imager Z2 microscope using Zen image capture software (Carl Zeiss Canada, Toronto, Ontario, Canada), and a Zeiss 710 laser scanning confocal microscope using ZEN 2010 image capture and analysis software. Data from wide-field and confocal microscopes were collected either as single scan images or z-stack images with multiple scans capturing a thickness of 2 to 7 μm of tissue at z scanning intervals of typically 0.4 to 0.6 μm. Final images were assembled using CorelDraw Graphics (Corel Corp., Ottawa, Canada) and Adobe Photoshop CS software (Adobe Systems, San Jose, CA, USA). Movie files were constructed using Zeiss ZEN software.

Cochlear ablation

Eight adult male Sprague-Dawley rats were taken for surgical procedures as previously described (Nagy et al., 2013), involving ablation of the cochlea and the spiral ganglion, which is the source of primary afferents innervating the cochlear nucleus. Rats were anesthetized with isofluorane, placed on a lateral supine position, and incisions were made into the external auditory canal using a lateral approach to expose the tympanic bulla lying lateral and superior to the digastric muscle. Once the tympanic bulla was visualized, a drill was used to expose the cochlea, which was ablated effectively producing a Scarpa ganglionectomy. Ganglion ablation was approached by cauterization in the area of the internal auditory meatus using a high temperature, fine tip, extended shaft micro-ophthalmic cauterization device (Bovie Medical Corp., Clearwater, Florida, USA), or by penetrating this area using a small hooked needle to ablate Scarpa's ganglion at its attachment to the

proximal end of the vestibular nerve. The surgical site was packed with haemostatic agent Avitene, sutured, and animals were maintained for a survival time of 7-9 days, during which time they were able to locomote and feed. Pain was controlled with buprenorphine (intramuscular, 0.03-0.06 ml/kg) every 8 hours for two days post-surgery. Tissues from animals subject to surgery were prepared for immunohistochemistry as described above. The intact side of each animal served as the basis for comparison of the effect of deafferentation on the contralateral lesion side, and possible effects of the surgery on the contralateral intact side was evaluated by comparison of the intact side with unoperated control animals.

Unilateral cochlear ablation led to a large loss of labelling for vglut1 and Cx36 in the ventral cochlear nuclei on the lesioned side. The loss of vglut1 was nearly complete, and therefore was not examined quantitatively. Loss of Cx36 was evaluated by counting the number of Cx36-puncta associated with individual neuronal somata in the ventral cochlear nuclei on the control *vs.* lesioned side in each of the eight animals taken for cochlear ablation. High magnification confocal images were taken of individual, blue Nissl counterstained, neuronal somata using single scans to allow visualization of distinct Cx36-puncta. A total of twenty somata were photographed on each of the control and lesioned sides in each of the eight animals, giving a total of 320 somata that were examined. The Cx36-puncta associated with somata were counted manually and the average number of puncta on somata on the control side *vs.* the lesioned side was expressed as mean ± s.e.m. as well as the percentage reduction (± s.e.m.) of the average of those on somata on lesioned *vs.* the control side. This percentage reduction on the lesioned side was calculated for each animal and thus served to normalize for variation in quality of labelling for Cx36 between animals. The average percentage reduction over the eight animals was then calculated. Cx36-puncta on a total of 163 neurons and 160 neurons were examined on the control side *vs.* lesioned side, respectively, in the eight animals with cochlear ablations, with an average of 20 neurons examined per side. A total of 4,365 puncta and 772 puncta were counted on the control *vs.* lesioned side, respectively, for an average of 545 on the control side *vs.*97 on the lesioned side.

RESULTS

Technical considerations

Robust immunofluorescence labelling of Cx36 is readily achieved with the commercially available anti-Cx36 antibodies used in this report. Several methodological points, however, warrant emphasis. First, we have repeatedly noted that optimal immunofluorescence labelling with these antibodies is highly dependent on appropriate tissue fixation conditions, because detection of Cx36 appears to be notoriously sensitive to fixation (Nagy, 2012; Nagy et al., 2013; Bautista and Nagy, 2014; Bautista et al., 2014). Labelling of Cx36 is best with a 1% formaldehyde/picric acid fix, is significantly diminished with a 2% concentration of this fix, and is obliterated with a 4% concentration. Even after perfusion with the 1% fixation, a perfusion flush of the fixative with non-fixative solution is recommended to avoid excessive post-fixation following tissue extraction. Others have also failed to detect labelling for Cx36 after strong tissue fixation, specifically in the cochlear nucleus of mouse (Howowitz et al., 2008). Second, this requirement for weak fixation precludes use of free-floating sections for immunohistochemical processing, because these sections tend to disintegrate upon repeated

handling. The use of cryostat sections is advisable, with optimal thickness of 10-20 μm; labelling of Cx36 is reduced in thicker sections despite the use of permeabilizing agents. In the event of a poor transcardiac perfusion with fixative, sections mounted on gelatinized slides or commercially available treated slides may occasionally deteriorate or dislodge from slides, which can be prevented by immersion of slide-mounted sections into 1% fixative for 15-45 sec prior to tissue processing, with only a slight loss of Cx36 immunolabelling quality. Third, this sensitivity to fixation can be particularly problematic when preparing fixative by depolymerization of paraformaldehyde. We have found that different batches of paraformaldehyde obtained from different commercial suppliers vary notoriously in their capacity to depolymerize, thus introducing variability in free aldehyde concentration and hence fixation strength. The problem can be surmounted by using commercially available depolymerized formaldehyde provided in sealed ampules, as described in Experimental Procedures above. Fourth, optimal labelling of Cx36 with weak fixation can be a advantages in double labelling approaches where detection of the second antigen is equally sensitive to fixation as Cx36, or this can be a disadvantage when the second antigen requires a strong fixation (*e.g.*,2-4% formaldehyde), as we have experienced in the case of double-labelling of Cx36 with such proteins as parvalbumin, calbindin, EGFP and (vglut1). This incompatibility in fixation can be partly overcome by introducing a short post-fixation of 30 min after perfusion with 1% fix and/or by varying perfusion volume with this fix (*e.g.*, 40 to 60 ml for a 30 gram mouse, 100 to 300 ml for a 300 gram rat). With these points in mind, we present here a description of Cx36 localization in some of the major auditory centers in ascending sequence of the auditory pathway.

Extensive distribution of Cx36 in the cochlear nuclei

Subdivisions of the cochlear nuclei include the prominent anteroventral nucleus (AVCN), the smaller posteroventral nucleus (PVCN), and the dorsal cochlear nucleus (DCN) extending as a thinner dorsolateral shell along the length of these other two nuclei. Immunofluorescence labelling of Cx36 was heterogeneously distributed in each of these regions but, among the auditory centers examined here, the ventral cochlear nuclei exhibited the highest density and the most remarkable patterns of Cx36 labelling. Low magnification overviews of labelling in Nissl counterstained (blue) sections of the AVCN in rat and the PVCN in mouse are shown in Figures 1A and 1B, respectively. In the AVCN, immunolabelling was most pronounced in the ventromedial portion of the nucleus, as well as near the 8^{th} nerve root entry zone and more dorsally along the entering root, and was sparse in the dorsolateral quadrant of the AVCN. Labelling was invariably associated with fluorescence Nissl-stained neurons, as seen in overlay (Fig. 1A3), but immunofluorescence was of sufficient intensity and density to outline the location and distribution of Cx36-immunopositive neurons even in the absence of Nissl staining. Immunolabelling was conspicuously and largely localized to neuronal somata and their initial dendrites, and only very rarely scattered in neuropil. The distribution of labelling for Cx36 was somewhat more sparse in the PVCN, where labelling was most concentrated on what appeared to be octopus cells (Fig. 1B). The distribution and characteristics of labelling for Cx36 in mouse AVCN (as well as all other auditory centers of mouse) resembled that observed in rat (Fig. 2A). Specificity of anti-Cx36 antibody was confirmed by comparisons of labelling in wide-type

vs. Cx36 knockout mice, where there was a total loss of immunofluorescence signal following Cx36 gene ablation (Fig. 2B).

The ventral cochlear nuclei contain several anatomically and physiologically well-characterized neuron types, including spherical and globular bushy cells, multipolar cells (aka, stellate or chopper cells) and octopus cells (for review see Cant and Benson, 2003; Trettel and Morest, 2001). In addition, located within the ascending portion of the 8th nerve bundle separating the AVCN and PVCN, as well as within the areas of the 8th nerve root, are clusters of relatively large cochlear root neurons (Merchán et al., 1988). Assignment of Cx36 expression to these and various other classes of cochlear neurons in the absence of definitive markers for each class is not possible. However, some classes of Cx36-positive neurons could be readily deduced based on the size of their somata in Nissl stained sections, their dendritic arborizations as revealed by associated labelling of Cx36, and/or their location within the cochlear nuclei complex. Labelling patterns displayed by some of these neuron types is shown in Figure 3. Though not evident at low magnification (Fig. 1), antibody labelling of Cx36 appears exclusively as immunofluorescence puncta (referred to here as Cx36-puncta), at least under the immunohistochemical protocols used here, which is qualitatively similar to the Cx36-puncta we detect in other CNS areas of mammals and fish (Curti et al., 2012; Nagy, 2012; Nagy et al., 2013; Bautista and Nagy, 2014; Bautista et al., 2014; Rash et al., 2014). Cx36-puncta are localized to the surface or periphery (*i.e.*, plasma membranes) of neuronal cell bodies and dendrites, as determined by confocal scanning through individual cells in the z-dimension. Intracellular labelling appears to be absent, perhaps due to masking of Cx36 epitopes during its trafficking to gap junctions and/or to low intracellular levels undergoing such trafficking. As discussed above (see Introduction), these Cx36-puncta are considered to reflect sites of gap junctions at close neuronal plasma membrane appositions.

In general, cellular distribution patterns of Cx36-puncta could be classified into three categories in the cochlear nuclei and other auditory regions examined. First is localization of these puncta at appositions between neuronal somata, which has been observed elsewhere (Curti et al., 2012; Bautista and Nagy, 2014), but is otherwise relatively rare in the mammalian CNS, where most neuronal gap junctions occur along arborizations of dendrites. In the present work, this pattern was observed only in the AVCN, and specifically with Cx36-puncta localized at appositions between cells having the appearance of bushy cells (Fig. 3A). Pairs of bushy cells were most frequently seen to be coupled by these puncta, but three or four cells linked in sequence by these puncta were also occasionally found (Fig. 3A). The second pattern, evident in both AVCN and PVCN, as well as in several other auditory centers, is represented by individual Cx36-puncta that were relatively uniform in size and were more or less uniformly distributed at the surface of neuronal somata and/or initial dendrites. This pattern was most strikingly associated with large multipolar neurons in the posterior portion of the AVCN (Fig. 3B,C), with octopus cells in the PVCN (Fig. 3D), and with what appeared to be the majority of auditory root neurons (Fig. 3E). The third pattern is well illustrated by labelling in the DCN, where Cx36-puncta were dispersed at moderate density throughout its superficial molecular layer and equally dispersed with low density in its deeper layers (Fig. 3F). These puncta were not associated with neuronal

somata (not shown), and their localization to fine dendritic processes was often precluded by poor fluorescence Nissl counterstaining of such processes in weakly fixed tissue.

EGFP reporter for Cx36 expression in the cochlear nuclei

Several transgenic mouse lines have been developed where protein reporter expression is driven by the Cx36 promoter (Degen et al., 2004; Wellershaus et al., 2007; Martin et al., 2011), providing potentially powerful models for delineation of neurons that produce Cx36 and presumably form electrical synapses composed of this connexin. So far, however, these mice have yet to be used for comprehensive documentation of neuronal populations with capability for Cx36 expression in widespread areas of the CNS. In the absence of such documentation, and due to possibilities of false-negative and false-positive reporter expression, it is not yet clear how reliably reporter expressed in cells of these mice corresponds to neurons that are known to express Cx36 or that are known to be electrically coupled. Here, we compare immunofluorescence detection of EGFP in EGFP-Cx36 mice with the distribution of immunolabelling for Cx36. In the AVCN and PVCN, neurons faintly to intensely immunopositive for EGFP in these mice (Fig. 4A1, 4B1) were similarly distributed as those labelled for Cx36 (Fig. 1). Double immunofluorescence labelling of EGFP combined with labelling for calbindin (Fig. 4A2, 4B2), which has been shown to be localized to cells having the morphological appearance of bushy cells (globular bushy cells) in the AVCN, multipolar and octopus cells in the PVCN and cartwheel cells in the DCN (Brazwinsky et al., 2008; Friauf, 1994; Zettel et al., 1991), revealed a high degree of EGFP/calbindin co-localization within what appeared to be bushy cells in the AVCN (Fig. 4A3) and in the ventral PVCN (Fig. 4B3). A more exact identification of EGFP-positive cell types was difficult due to poor labelling of EGFP along dendritic processes (Fig. 4C) and, hence, poor definition of their morphology. Some cells in the granular cell domain are positive for EGFP and negative for calbindin (Fig 4A, B), and they are negative for Cx36 labelling (Fig. 1). In addition, octopus cells appear negative for calbindin (Fig. 4B), but these cells have been shown to express calbindin in rats (Friauf, 1994).

Labelling for EGFP in the DCN was somewhat more robust in neuronal somata, although dendritic arborizations were weakly labelled (Fig. 4D-F). EGFP-immunopositive neurons were distributed in all regions of the DCN, with small cells having diameters of 6-10 μm localized in the molecular layer, and larger cells with long axis diameters of 20-25 μm concentrated along the fusiform cell layer and sparsely distributed in deeper layers (Fig. (4D-G)). Among those EGFP-positive cells, we identified superficial stellate cells within the molecular layer and fusiform cells in the fusiform cell layer. Double immunolabelling for EGFP combined with calbindin, which is a marker for cartwheel cells in the rodent DCN (Friauf, 1994), showed that all EGFP-positive cells were devoid of labelling for calbindin (Fig. 4F). Separate animals subject to tissue fixation with 2% formaldehyde-picric acid were taken for attempts to double-label for Cx36 and EGFP. Despite the incompatibility of fixative strengths required for optimal labelling of these proteins, some Cx36-puncta within the molecular layer (Fig. 4H1) were found to be localized along the primary dendrites of large EGFP-positive neurons likely corresponding to fusiform cells (Fig. 4H2). Similar attempts to localize Cx36-puncta along EGFP-positive dendrites, and specifically at

dendritic appositions, in the molecular failed due to inadequate labelling of EGFP along fine dendritic processes.

Cx36 at vglut1-containing axon terminals in cochlear nuclei

In fish, 8th cranial nerve primary afferent fibers terminating in the brainstem are know to form mixed synapses, where the terminals of these afferents transmit not only chemically, but also electrically via gap junctions formed by Cx35, which is the fish ortholog of Cx36 (Rash et al., 2003, 2013). Recently, we have reported that Cx36 is similarly localized to nerve terminals of 8th nerve primary afferents ending on neurons in the vestibular nuclei, forming morphologically mixed synapses (Nagy et al., 2013). Such synapses have been observed ultrastructurally in the ventral cochlear nuclei of rat, where large nerve terminals laden with synaptic vesicles were seen forming clearly identified gap junctions with unidentified postsynaptic neurons (Fig. 5), and it was suggested that these terminals may be of primary afferent origin (Sotelo and Triller, 1982). In the cochlear nuclei, the size and locations of many of the neurons displaying Cx36-puncta suggest that they could receive auditory nerve input, and several of the neuron types that we found to be decorated by these puncta (*e.g.*, bushy, multipolar, octopus and auditory root neurons) are known to be innervated by 8th nerve afferent terminals, raising the possibility that Cx36 may be localized to these terminals. This was examined by double immunofluorescence localization of Cx36 in relation to vglut1, which is a specific marker of excitatory synapses, including those formed by auditory nerve terminals (Gómez-Nieto and Rubio, 2009).

Double labelling for these proteins in the AVCN of rat and mouse is shown in Figures 6-8. Immunolabelling for vglut1 in the cochlear nucleus resembled that in previous studies of guinea pig and rats (Gómez-Nieto and Rubio, 2009; Zhou et al., 2007), but was more variable from animal to animal, particularly in mouse, due to less than optimal fixation for vglut1, but which was required to simultaneously label Cx36. In mouse, labelling of Cx36 in the AVCN (Fig. 6A) had a similar punctate appearance as seen in rat (Fig. 2), Cx36 was associated with many though not all neuronal somata, and Cx36-puncta around individual neurons showed a high degree of co-localization with vglut1 (Fig. 6B). This co-localization was more extensively examined in more robustly labelled sections from rat (Fig. 7 and 8). At low magnification, many neuronal somata were heavily surrounded by labelling for vglut1 (Fig. 7A1), and nearly all neurons that were heavily labelled for Cx36 on their somata and proximal dendrites (Fig. 7A2) were also densely decorated with vglut1-positive axon terminals, as seen in the AVCN and along the course of auditory root neurons (Fig. 7A3, red/green overlap appears as yellow in overlay). Neurons in the dorsolateral area of the AVCN lacking Cx36 were nevertheless densely innervated by vglut1-positive terminals.

Higher magnification confocal analysis of individual neuronal somata revealed that collections of Cx36-puncta on these somata were often associated with patches of labelling for vglut1, as shown by examples of two AVCN neurons (Fig. 8A, B) and a auditory root neuron (Fig. 8C). A similarly dense distribution of vglut1-positive terminals was seen on the somata and initial dendritic segments of octopus cells in the PVCN (Fig. 8D1), and Cx36-puncta typically concentrated on these cells (Fig. 8D2) were invariably localized to these terminals (Fig. 8D3). Surrounding terminals lacking association with these neurons were

devoid of Cx36-puncta (Fig. 8D). Images in Fig. 8A and 8D3 are presented as Neuroimage file 1 and 2. This Cx36/vglut1 association suggests localization of Cx36-containing gap junctions at sites where vglut1-positive terminals form synaptic contacts with neuronal somata and proximal dendrites, presumably reflecting sites of morphologically mixed synapses. It is of note that Cx36-puncta in the DCN were never found to be co-localized with terminal boutons labelled for either vglut1 or vglut2 in the molecular layer or deeper layers.

Cx36 at purely electrical synapses

In the course of examining Cx36/vglut1 relationships, our attention was drawn to one of the three categories of labelling for Cx36 described above, namely, localization of Cx36 at appositions between medium sized neurons in the central and ventral portions of the AVCN that was shown in Figure 3A. The identity of these neurons is not entirely certain, but several anatomical and molecular parameters allowed their tentative designation as bushy cells. These parameters include, their location within the AVCN, the medium size of their cell body, the endbuld-like appearance of vglut1 labelling (Fig. 9F), and their labelling for calbindin, which is a marker for at least one type of bushy cell (Brazwinsky et al., 2008; Zettel et al., 1991). In both rat and mouse tissues, bushy cells were only poorly labelled for calbindin, likely as a result of our use of weak fixation (Fig. 4, 9A), but double-labelling showed that these calbindin-positive neurons harbour Cx36-puncta at their somatic appositions (Fig. 9A). Double-labelling for Cx36 and vglut1 associated with these neurons (Fig. 9B1), together with labelling of Cx36 in the same sections counterstained with blue Nissl (Fig. 9B2), showed that vglut1-positive terminals were heavily concentrated around their somata and that Cx36-puncta at their somatic appositions were not co-localized with vglut1 (Fig. 9B). This is shown by higher magnification confocal analysis in Figures 9C-F. It is of note that in separate sections double-labelled for Cx36 and vglut2, Cx36-puncta localized at sites of somatic appositions were similarly lacking co-localization with vglut2 (not shown).

In Figure 9C, the somata and short initial dendritic segments of two neurons and a portion of a third are delineated by labelling of Cx36 and vglut1 around their periphery. As in the case of other cells described above, Cx36 is frequently seen overlapping or in close association with labelling of vglut1-positive terminal boutons. Labelling of Cx36 at sites of somatic appositions consisted of numerous Cx36-puncta (~18 in the example of Fig. 9C), and these sites were devoid of labelling for vglut1, despite the occurrence of substantial Cx36/vglut1 co-localization in immediately adjacent regions (Fig. 9D, E). Arrays of Cx36-puncta at these somatic appositions could be visualized: i) edge on where they appeared as linear arrangements of unresolved puncta (Fig. 9D); ii) at a slightly oblique angle where Cx36-puncta become somewhat discernable (Fig. 9E); or iii) en face where the size of the appositions and full complement of Cx36-puncta (> 30 puncta in 9F) become readily apparent (Fig. 9F). These results suggest that a population of bushy cells receive morphologically mixed synapses formed by vglut1-positive terminals and are at the same time coupled by purely electrical synapses formed by Cx36-containing gap junctions.

Primary afferent source of Cx36 associated with vglut1

Unilateral ablation of the cochlea was conducted on rats to determine whether vglut1-positive axon terminals bearing Cx36-puncta in the cochlear nuclei arise from 8th nerve primary afferents originating from neurons in the spiral ganglia. All eight animals subject to this procedure exhibited a near total depletion of labelling for vglut1 in the ventral cochlear nuclei, as shown by comparison of vglut1 detection on the unoperated control side in the AVCN (Fig. 10A) *vs.* the contralateral lesioned side (Fig. 10B). This massive loss of vglut1 was accompanied by a large loss of labelling for Cx36 around neuronal somata and their proximal dendrites in these nuclei, as shown in similar sections of the AVCN on the control side (Fig. 10C) *vs.* the lesioned contralateral side (Fig. 10D). Auditory root neurons were equally depleted of their contacts by vglut1-containing nerve terminals (not shown), which was paralleled by a near total loss of labelling for Cx36 associated with these neurons, as shown by comparison of the density of Cx36-puncta on root neurons on the intact (Fig. 10E) *vs.* lesioned (Fig. 10F) side. Counts of Cx36-puncta associated with individual neuronal somata on the control intact side *vs.* puncta associated with somata on the lesioned side indicated an average reduction of 81 ± 3.2%, based on an average of 27 ± 2.6 puncta per somata on the control side *vs.* 5.0 ± 1.1 puncta on somata on the lesioned side. Examples of images used for counts of Cx36-puncta on the intact side and those remaining on the lesioned side are shown in Figure. 10G and 10H, respectively.

Cochlear ablation had no discernable effect on labelling for Cx36 or vglut1 in the most superficial layer of the DCN on the lesioned side (not shown). Labelling of Cx36 and vglut1 were also unaffected in the ventral cochlear nuclei on the unoperated side, including those areas of the AVCN where neuronal somata were seen linked by Cx36-puncta at their appositions (Fig. 11A). Similar areas on the lesioned side showed a large loss of both vglut1-positive terminals (Fig. 11B1) and Cx36-puncta (Fig. 11B2) that normally surround the somata of these neurons. However, Cx36-puncta at somatic appositions between these neurons was preserved on the lesioned side, as shown at low magnification (Fig. 11B2) and at higher confocal magnification with blue Nissl counterstaining (Fig. 11C). The loss of vglut1-containing terminals in the ventral cochlear nuclei following cochlear ablation indicates that all or nearly all of these terminals are of primary afferent origin, and the loss of the bulk of Cx36-puncta accompanying the degeneration of these terminals is consistent with localization of Cx36 at these primary afferent terminals forming morphologically mixed synapses. In contrast, the persistence of Cx36 at cell-cell contacts after cochlear ablation is consistent with its localization at gap junctions forming purely electrical synapses at these contacts.

Cx36 in other nuclei of the ascending auditory pathway

Medial nucleus of the trapezoid body (MNTB)—A second prominent nucleus in the auditory pathway is the MNTB. Neurons in this structure receive inputs from bushy (*i.e.*, globular-bushy) neurons in the AVCN and project to the lateral superior olivary nucleus (LSO). Among all CNS regions, afferents to MNTB from the AVCN are distinctive because they terminate as massive endings nearly engulfing the whole of MNTB neuronal somata, forming their classic calyx of Held innervation pattern in this structure (Sätzler et al., 2002; Rollenhagen and Lubke, 2006). Immunofluorescence labelling of Cx36 in the MNTB was as

striking as that observed in the cochlear nuclei. Here, we show images of MNTB from mouse (Fig. 12), but similar labelling patterns of Cx36 were observed in this structure of rat (not shown). Low magnification comparisons of labelling for vglut1 and Cx36 with blue Nissl counterstaining is shown in Figure 12A. Although not examined in detail or quantitatively, the somata of most large neurons 18-25 μm in diameter were heavily invested with calyx-like labelling for vglut1 and, conversely, nearly all of the vglut1 labelling in MNTB was associated with these large neurons; smaller neurons 10-15 μm in diameter were present, but displayed little or no association with vglut1 (compare vglut1 in Fig. 12A1 with same Nissl stained section in 12A2). This pattern of labelling for vglut1 was paralleled nearly exactly by an overlapping pattern of rich labelling for Cx36 (Fig. 12A2, A3). As shown at higher magnification (Fig. 12B), Cx36 (labelled red) was detected exclusively as Cx36-puncta of relatively uniform size localized to the surface (periphery) of cells, and intracellular red fluorescence in neurons bearing these puncta was not discernably different in sections from wild-type *vs.* Cx36 ko mice (not shown). Cx36-puncta were often co-localized with vglut1, as seen at low magnification (Fig. 12A3) and at higher confocal magnification (Fig. 12B3, 12C and 12D). It is of note that, despite an extensive search, Cx36-puncta were not observed at appositions between MNTB neuronal somata; in fact, these somata were rarely found to be in apposition to each other. Further, although not examined quantitatively, it appeared that cochlear ablation had little effect on the density or immunofluorescence intensity of Cx36-puncta localized on MNTB neurons (not shown).

In EGFP-Cx36 mice, large MNTB neuronal somata were surrounded by calyx-like labelling for EFGP (Fig. 13A1), which matched the distribution of vglut1 labelling around these same neurons counterstained with blue fluorescence Nissl (Fig. 13A2), as seen by image overlay (Fig. 13A3). Confocal analysis indicated that this EGFP labelling on MNTB neuronal somata (Fig. 13B1) was co-localized with vglut1 (Fig. 13B2), as seen in image overlay (Fig. 13B3), suggesting transport of EGFP from EGFP-positive bushy cells to their terminals on MNTB neurons. Other sites of such EGFP transport might have therefore been expected, but the MNTB was the only location in the auditory regions presently examined where evidence was found for EGFP transport to and localization in terminals. These and the above results suggest localization of EGFP reporter for Cx36 as well as Cx36-puncta at vglut1-positive calyx of Held terminations formed by bushy cell afferents on MNTB neurons.

Superior olivary complex (SOC)—The SOC is ventrally located in the brainstem and it is formed by a collection of nuclei that mainly receive ipsilateral excitatory innervation from bushy (spherical- and globular-bushy) cells of the AVCN and inhibitory inputs from the MNTB. The major SOC nuclei are the lateral superior olivary complex (LSO), the medial olivary nuclei (MSO), the MNTB (described above) and the periolivary nuclei. The LSO consists of large fusiform-bipolar neurons in the center and distinctive large cells around the LSO periphery (periolivary neurons) (Schofield and Cant, 1992; Thompson and Schofield, 2000). The MSO is a collection of bipolar neurons located medial to the LSO. Neurons in the central region of the LSO were devoid of labelling for Cx36, whereas moderate numbers of Cx36-immunopositive neurons were clearly seen scattered around the periphery of the nucleus, as shown in mouse LSO in Figure 14A. A similar pattern of labelling for Cx36 was seen in regions of the LSO in rat, where distinctive neuronal somata with long axis

diameters of 25 μm flanking the LSO (Fig. 14B1) were often labelled for Cx36, as shown in lateral periolivary areas (Fig. 14B2). Higher magnification showed that labelling Cx36 concentrated at the boundaries of the LSO consisted, as elsewhere in the brain, exclusively of Cx36-puncta, which were associated with neuronal somata and their initial dendritic segments (Fig. 14C), similar to labelling patterns seen in the ventral cochlear nuclei, except at a lower density. Neuronal somata and their initial dendrites were rarely seen adjacent to each other, and no instances were encountered of Cx36-puncta localization at such appositions. Double immunolabelling for Cx36 and vglut1 showed that the vast majority of Cx36-puncta decorating the somata and initial dendrites of neurons at the LSO peripheral margins were co-localized with vglut1 (Fig. 14C2, inset).

In EGFP-Cx36 mice, cells within the LSO displayed only background fluorescence that was observed with anti-EGFP antibody omission, while EGFP-positive neuronal somata were observed at the boundaries of the nucleus, as shown at its lateral regions (Fig. 14D1) corresponding to a similar field as shown in rat (Fig 14B). In rare instances, the weak and strong fixations required for visualization of labelling for Cx36 and EGFP struck a fortuitous compromise, and in this case revealed the association of labelling for Cx36 (Fig. 14D2) on the very same neurons that were positive for EGFP (Fig. 14D1), as seen in overlay images (Fig. 14D3).

No labelling of Cx36 was observed in the MSO (not shown), which was unlikely a false-negative outcome because MSO neurons were entirely devoid of Cx36-puncta in sections where neurons in MNTB and those surrounding the LSO in the vicinity of the MSO were well labelled for Cx36.

Dorsal nucleus of the lateral lemniscus (DLL) and nucleus sagulum—The DLL receives input from lower auditory nuclei (DCN, LSO) and projects bilaterally to the inferior colliculus and contralaterally to the DLL (Thompson and Schofield, 2000). The nucleus sagulum also projects to the inferior colliculus. In the DLL of mouse, a high proportion of large neuronal somata displayed heterogeneous labelling for Cx36 ranging from sparse to dense (Fig. 15A), while labelling in the nucleus sagulum was sparsely distributed in medial portions of the nucleus (Fig. 15B). In both nuclei, Cx36-puncta were heavily concentrated on some large neuronal somata and their initial dendrites (Fig. 15C, D), while these puncta were more sparsely distributed or were absent on smaller neuronal somata. As in the LSO and MNTB, Cx36-puncta were never clearly observed at appositions between neuronal elements either in the DLL or the nucleus sagulum. Qualitatively similar though a lower density of labelling was observed in these two nuclei of rat (not shown).

In EGFP-Cx36 mice, the DLL showed intense labelling for EGFP in neuronal cell bodies with poor labelling of their dendrites, and dense collections EGFP-positive dorsoventrally oriented axons were seen in regions dorsal to the nucleus (Fig. 15E, F). In the nucleus sagulum, EGFP labelling was observed in a subpopulation of neurons, as shown with Nissl counterstaining (Fig. 16G). Numerous attempts to achieve adequate labelling for Cx36 in combination with labelling for vglut1 in the DLL and nucleus sagulum failed in both rat and mouse. It is of note, however, that stronger fixations resulting in obliteration of labelling for

Cx36 did produce robust labelling of vglut1 that appeared to be associated with terminal boutons in both the DLL and the nucleus sagulum (not shown).

Cx36-puncta and EGFP-positive neurons were extremely sparse or absent in most of many sections through the intermediate nucleus of the lateral lemniscus, and were absent in the ventral nucleus of the lateral lemniscus (not shown).

***Inferior colliculus* (IC)—**The inferior colliculus is the principal midbrain nucleus of the auditory pathway and receives input from several peripheral brainstem nuclei in the auditory pathway, as well as inputs from the auditory cortex. The inferior colliculus has three subdivisions: the central nucleus (CNIC), a dorsal cortex (DCIC) that surrounds the CNIC dorsally, and an external cortex (ECIC) that is located lateral to the CNIC, and has been alternatively referred to as the ventrolateral nucleus (Loftus et al., 2008). In the IC of adult rat, labelling of Cx36 was of sparse to moderate density in each of its major subdivisions (Fig. 16A-C), and consisted of widely distributed Cx36-puncta that were mostly of fine calibre in the DCIC (Fig. 16A), CNIC (Fig. 16B) and dorsal region of the ECIC (not shown), and that displayed a greater fluorescence intensity in ventral regions of the ECIC (Fig. 16C). In fluorescence Nissl stained sections, Cx36-puncta were not found to be distributed on the surface of neuronal somata (not shown) and, after an extensive search, none were found to be co-localized with labelling for vglut1 (not shown). In EGFP-Cx36 mice with Nissl counterstaining, the inferior colliculus showed considerable regional heterogeneity in the density of EGFP-immunopositive neurons. The highest density was clearly evident in the medial portion of the DCIC, where blue Nissl counterstaining reveal labelling of EGFP in a subpopulation of neurons (Fig. 16D). EGFP-positive neurons were very sparsely distributed in anterior regions of the CNIC (Fig. 16E), and were present at moderate levels in posterior areas of the CNIC, where EGFP was localized in a subpopulation of small neurons and a few larger neurons (Fig. 16F). The ECIC displayed a large difference in the density and characteristics of EGFP-positive neurons in its dorsal *vs.* ventral regions. These neurons in dorsal areas were small and of low density similar to that in the CNIC (Fig. 16G), whereas ventral areas contained an array of larger EGFP-positive neurons (Fig. 16H). More ventral to the ECIC, the lateral lemniscus contained dense collection of EGFP-positive fibers that appeared to be entering the inferior colliculus (Fig. 16I).

Medial geniculate nucleus and auditory cortex—The medial geniculate in the thalamus receives the majority of the ascending input from the inferior colliculus and descending input from the auditory cortex. Like several other thalamic nuclei (*e.g.,* the lateral geniculate nucleus, posterior thalamic nuclear group), the medial geniculate nucleus was remarkably devoid of labelling for Cx36, as shown in its ventromedial portion adjacent to the posterior thalamic triangular nucleus, which contained sparse Cx36-puncta and is shown as a positive control for Cx36 detection (Fig. 17A).

Lastly, we examined Cx36 expression in the primary auditory cortex, which receives ascending input from the medial geniculate. In this cortical area, Cx36-puncta were barely detectable in layer I, were very sparse in layer II, and sparse in layer III (Fig.17B). In deeper layers (IV-VI), Cx36-puncta were distributed at moderate density in layer IV and V,

appeared to be somewhat more concentrated in the midregion of layer V, and were of slightly lower density in layer VI (Fig. 17B). The distribution of Cx36-puncta in auditory cortex was similar to that in other cortical regions, notwithstanding possible slight difference in their overall density, and further in depth analysis was not conducted here, as this would best be addressed in the context of studies of Cx36 in cerebral cortical areas in general.

Note on EGFP as a reporter for Cx36 expression

In the EGFP-Cx36 line of mice used here, there are so far only a few reports indicating a reasonable correlation between neurons that express EGFP and those that are known to form ultrastructurally-identified gap junctions and/or are known to be electrically coupled (Bautista and Nagy, 2014; Palacios-Prado et al., 2014). However, we have found similarly high correlations in dozens of other brain regions (Nagy, unpublished observations). Still, there is reason for caution: do as many of the remarkably abundant EGFP-positive neurons as we observe throughout the CNS of EGFP-Cx36 mice truly express Cx36, or are there cases of false-positive EGFP expression in these mice? This question could most practically be addressed by technical improvements in simultaneous immunolabelling for Cx36 and EGFP. In these mice, we have not yet examined systematically the more readily discernibly alternative of false-negative EGFP expression in cells known to be electrically coupled, but expect that instances of this will appear based on the stark absence of EGFP in neurons that in the entire CNS are premier for their abundance of gap junctions and documented electrical coupling (Devor and Yarom, 2002; Leznik and Llinas, 2005; Hoge et al., 2011), namely those in the inferior olivary nucleus (Nagy, unpublished observations).

In the auditory system, our findings provide a direct correlation of Cx36-puncta appearing on EGFP-positive neurons in two areas, namely the DCN and the peri-regional LSO. In other regions, identified neuron types decorated with Cx36-puncta were, in separately processed sections, clearly labelled for EGFP, including fusiform cells and what in all likelihood were superficial stellate cells in the DCN, as well as bushy cells, octopus and auditory root neurons in the ventral cochlear nuclei. In the remaining upstream auditory nuclei, except for the MNTB, it was not possible to assign both Cx36 (*i.e.*, Cx36-puncta) and EGFP expression to any particular neuronal type. In the MNTB, all or nearly all large presumably principal neuronal somata displayed Cx36-puncta as well as what appeared to be terminal contacts positive for EGFP, however, the somata themselves were weakly labelled for EGFP, suggesting in this case a poor correlation between robust Cx36 and EGFP expression.

DISCUSSION

Based on immunofluorescence visualization of Cx36 as a marker for cellular sites of Cx36-containing neuronal gap junctions and immunolabelling of EGFP as a reporter for Cx36 expression, we present evidence indicating the potential for electrical synaptic transmission in multiple centers of the auditory system and between multiple types of neurons within these centers. Our results leave open a host of unanswered questions, not the least of which concerns the apparent diversity and complexity of neuronal gap junctions in some of the

main auditory nuclei and whether these junctions have functional correlates in electrical synaptic coupling.

Purely electrical *vs*. mixed synapses

Neurons can establish gap junctions between their dendrites, between somata, and between dendrites and somata, all of which we refer to as “purely electrical synapses”, whereas gap junctions between their axon terminals and postsynaptic elements contribute to the formation of “mixed synapses” that have the potential for dual chemical and electrical synaptic co-transmission (Bennett, 1972, 1974, 1977; Bennett and Goodenough, 1978). The two types of synapses are readily distinguished by ultrastructural identification of the participating gap junction-forming structures. By immunofluorescence labelling of Cx36 and appropriate cellular markers, Cx36-puncta representing gap junctions at neuronal somatic or dendritic appositions can be assigned with reasonable confidence to the class of purely electrical synapses in some systems (Hidaka et al., 2004; Curti et al., 2012; Bautista and Nagy, 2014; Baude et al., 2007). Immunofluorescence localization of Cx36-puncta to axon terminals can also reveal sites of mixed synapses, as in the case Cx36 associated with terminal boutons in the vestibular nuclei (Nagy et al., 2013). However, Cx36-puncta scattered in neuropil in many areas of the brain are often localized to purely electrical synapses between fine dendrites that are difficult to visualize by standard neuronal markers. Alternatively, a clear lack of association of these Cx36-puncta with axon terminal markers can by default exclude them as gap junction constituents of mixed synapses. Here, our results provide evidence for Cx36 localization at both purely electrical synapses and mixed synapses in the auditory system. As only Cx36 was examined in the present study, we cannot exclude the possibility that other connexins may also contribute to the formation of neuronal gap junctions in various auditory brain centers.

Cx36 at purely electrical synapses in the AVCN

In the AVCN, clusters of Cx36-puncta that lacked association with vglut1, that persisted after cochlear ablation, and that appeared at somatic appositions were in all likelihood gap junctions forming purely electrical synapses between bushy cells. This conclusion is consistent with our report of ultrastructurally characterized gap junctions between the somata of bushy cells in the rat AVCN (Gómez-Nieto and Rubio, 2009) as well as the AVCN of rhesus monkey (Gómez-Nieto and Rubio, 2011). The existence of somato-somatic and somato-dendritic gap junctions in the AVCN was reported much earlier by Sotelo and colleagues (Sotelo et al., 1976), but in this early study the cell types involved were not identified, though they too found that these gap junctions persisted after 8th nerve deafferentation.

The typically dozens of Cx36-puncta each representing a gap junction plaque at bushy cell somatic appositions suggests that coupling between these cells may be particularly strong. So far, however, electrical coupling between bushy cells has not been reported, and intracellular injections of biocytin, a tracer permeable to Cx36-containing gap junctions, has not been found to spread between bushy cells in studies of AVCN *in vitro* (Cao et al., 2007). It is of note that absence of dye- or tracer-coupling does not equate to absence of gap junctions or electrical coupling. Neurons well-established to be electrophysiologically

coupled by Cx36-containing gap junctions may nevertheless defy demonstrations of dye-coupling in some systems (Logan et al., 1996a,b; Gibson et al., 1999) or exhibit variability of such coupling (Curti et al., 2012), suggesting loss of junctional channel permeability to molecules, perhaps in the course of brain slice preparation, despite persistence of electrical coupling. In any case, demonstration of functional electrical synapses between bushy cells could contribute to an understanding of how synchronization of firing is enhanced among these cells, and in particular spherical-bushy cells, when compared to the corresponding somewhat less coordinated activity in their auditory nerve afferents (Joris et al., 1994a,b; Paolini et al., 2001; Joris and Smith, 2008). Given that synchronization of neuronal activity is a hallmark of properties conferred by electrical synapses (Bennett and Zukin, 2004; Connors and Long, 2004; Hormuzdi et al., 2004; Connors, 2009), networks of bushy cells electrically coupled by these synapses could respond in a synchronous fashion to activity in their auditory nerve inputs despite less than synchronous activity of these inputs to individual cells in the coupled network.

Purely electrical synapses in the DCN

The DCN contains several types of neurons, including inhibitory interneuron stellate and cartwheel cells in the superficial molecular layer, excitatory principal fusiform cells in the fusiform cell layer and other types in deeper layers (Browner and Baruch, 1982). The neuronal organization of the DCN is similar to the cerebellar cortex (Mugnaini, 1985; Wouterlood et al., 1984), where stellate cells form gap junctionally coupled networks (Mann-Metzer and Yarom, 1999; Mugnaini, 1985; Wouterlood et al., 1984). Recently, electrophysiological analysis in the DCN showed weak electrical coupling between stellate cells and strong electrical coupling between these cells and fusiform cells (Apostolides and Trussell, 2013). Although ultrastructural evidence of gap junctions between stellate and fusiform cells is lacking, our detection of Cx36-puncta in the DCN supports the existence of gap junctions composed of Cx36 within this structure, including their localization on primary dendrites of EGFP-positive neurons that may correspond to fusiform cells. So far, gap junction formation by axon terminals in the DCN has not been reported, consistent with our observations that Cx36-puncta in the DCN were not associated with either vglut1- or vglut2-containing terminals, including those that are likely auditory nerve endings in deep layers or that likely belong to parallel fiber endings in the molecular layer (Rubio et al., 2008). Overall, our results support ultrastructural and electrophysiological data (cited above) indicating the existence of electrical synapses within the molecular layer of the DCN. Functionally, electrical coupling between dendrites of fusiform cells and superficial stellate cells at this early stage of auditory processing has been suggested to allow the ongoing sensory input to bidirectionally regulate the threshold for recruitment of local inhibition (Apostolides and Trussell, 2013, 2014).

Mixed synapses in the auditory system

Decades ago, nerve terminals forming gap junctions with unidentified neuronal somata was reported in the ventral cochlear nuclei of rat, and it was suggested that these terminals may be of primary afferent origin (Sotelo and Triller, 1982). We now establish that these gap junctions are composed of Cx36, that they occur at terminals innervating multiple neuron types, including bushy cells, octopus cells, auditory root neurons and possibly others in the

ventral cochlear areas, and that they are indeed formed by terminals of primary afferent origin. In the case of bushy cells, with their high percentage of surface covered by primary afferent endbulbs of Held, it is almost certain that these gap junctions are formed by the endbulbs. The similarly distributed Cx36-puncta we found on neuronal somata in the MNTB and their co-localization with vglut1, together with the dense coverage and envelopment of these somata by calyx of Held terminations originating from AVCN globular bushy cells, strongly suggests the formation of Cx36-containing gap junctions by these calyceform terminations on MNTB neuronal somata. This is supported by expression of EGFP reporter for Cx36 in bushy cells and apparent transport of this EGFP to calyceform endings on MNTB neurons, where the EGFP was also co-localized with vglut1. Another location of Cx36 association with vglut1 was around neuronal somata located at peripheral margins of the LSO. In the DLL and nucleus sagulum, Cx36-puncta were distributed on neuronal cell bodies in patterns resembling those in other regions where similar puncta were co-localized with vglut1, suggesting that these puncta may also be associated with nerve terminals forming gap junctions with postsynaptic somata. However, technical limitations noted above precluded double labelling for Cx36 and vglut1 in these areas.

Identification of mixed synapses and demonstrations of their physiological importance in the CNS of lower vertebrates has a long history (Bennett, 1972, 1974, 1977; Bennett and Goodenough, 1978; Pereda et al., 2003, 2004). In mammalian CNS, evidence for mixed synapses has been found only at a few locations, including rat lateral vestibular nucleus (LVN) (Korn et al., 1973; Wylie, 1973; Sotelo and Korn, 1978; Nagy et al., 2013), spinal cord (Rash et al., 1996; Bautista et al., 2014) and hippocampus (Vivar et al., 2012; Nagy, 2012). The present findings suggest multiple additional sites where axon terminals form mixed synapses in the auditory system of mouse and rat. In the absence of evidence for an electrical component of transmission at such synapses, which so far includes most of those found in mammalian CNS, these may be referred to as “morphologically” mixed synapses, which is implicit in our discussion of these structures. Obtaining evidence for functionally mixed synapses might be a challenge, but two sites where putative mixed synapses occur, namely mossy fiber terminals in the posterior hippocampus of rat and the calyx of Held, are both amenable to electrophysiological recording from axon terminals (Alle et al., 2009; Forsythe, 1994; Borst et al., 1995), which could allow direct assessment of electrical coupling between pre- and postsynaptic elements by dual recording approaches.

The physiological relevance of mixed synapses (*i.e.*, those formed by nerve terminals) to integrative processing in mammalian systems has rarely been considered in mammalian systems. Speed of transmission at their putative electrical component appears not to be an advantage over speed of chemical transmission at mammalian body temperature (Bennett, 1972, 1977, 1997, 2000; Bennett and Goodenough, 1978), but this remains to be fully assessed in mammals. Alternatively, synchronization of neuronal activity could be a particularly important contribution of these synapses in the auditory system. In this regard, bushy cells appear to be unique in mammalian CNS because they appear to be the first clear example of cells that both receive mixed synapses and appear themselves to be coupled by purely electrical synapses. As has been demonstrated in lower vertebrates (Pappas and Bennett, 1966; Bennett et al., 1967; Kriebel et al., 1969; Korn et al., 1977) and discussed in

the context of the lateral vestibular nucleus in rat (Korn et al., 1973; Nagy et al., 2013), coupling between two neurons can be mediated by presynaptic fibers, which may occur in situations where a single fiber innervates and forms mixed synapses on two different neurons, allowing activity in one neuron to be transmitted to another via the gap junctions at each end of the collateral. This may occur in the auditory system because, among the cell types on which we find mixed synapses, individual cells can receive collateral inputs from single auditory afferents. In the AVCN, for example, fibers forming endbulb synapses on the soma of one bushy cell can form synapses on the dendrite of another bushy cell, the so called 'synaptic dyads' (Gómez-Nieto and Rubio, 2009, 2011). Further, we have found examples of one auditory ending synapsing with two bushy somata (Rubio, unpublished observations), which could allow electrical coupling of those cells by way of these presynaptic fibers, even further contributing to the potential for synchronous activity of bushy cells.

Supplementary Material

Refer to Web version on PubMed Central for supplementary material.

Acknowledgements

This work was supported by grants from the Canadian Institutes of Health Research and from the Natural Sciences and Engineering Research Council to J.I.N., by grants from the National Institutes of Health (NS31027, NS44010, NS44295) to J.E. Rash with subaward to J.I.N., and by grants from the NIH (1R01DC013048-01) and from internal funding by the Universty of Pittsburgh to M.E.R. We thank B. McLean for excellent technical assistance, Dr. D. Paul (Harvard University) for providing breeding pairs of Cx36 knockout mice and their wild-type counterparts, and Drs. W Bautista and B. Blakley for help with performing cochlear ablations.

Abbreviations

AVCN	anteroventral cochlear nucleus
CNS	central nervous system
Cx36	connexin36
CNIC	central nucleus of the inferior colliculus
DCIC	dorsal nucleus of the inferior colliculus
DCN	dorsal cochlear nucleus
DLL	dorsal nucleus of the lateral lemniscus
ECIC	external nucleus of the inferior colliculus
EGFP	enhanced green fluorescent protein
LSO	lateral superior olivary complex
MNTB	medial nucleus of the trapazoid body
PBS	phosphate-buffered saline
PVCN	posteroventral cochlear nucleus
SOC	superior olivary complex

TBS	50 mM Tris-HCl, pH 7.4, 1.5% NaCl
TBSTr	TBS containing 0.3% Triton X-100
vglut1	vesicular glutamate transporter-1

REFERENCES

Alle H, Roth A, Geiger JRP. Energy-efficient action potentials in hippocampal mossy fibers. Science. 2009; 326:1405–1408. [PubMed: 19745156]

Apostolides PF, Trussell LO. Regulation of interneuron excitability by gap junction coupling with principal cells. Nat Neurosci. 2013; 16:1764–1772. [PubMed: 24185427]

Apostolides PF, Trussell LO. Control of interneuron firing by subthreshold synaptic potentials in principal cells of the dorsal cochlear nucleus. Neuron. 2014; 83:324–330. [PubMed: 25002229]

Baude A, Bleasdale C, Dalezios Y, Somogyi P, Klausberger T. Immunoreactivity for the GABAa receptor 1 subunit, somatostatin and connexin36 distinguishes axoaxonic, basket and bistratified interneurons of the rat hippocampus. Cerebral Cortex. 2007; 17:2094–2107. [PubMed: 17122364]

Bautista W, Nagy JI, Dai Y, McCrea DA. Requirement of neuronal connexin36 in processes mediating presynaptic inhibition of low threshold afferents in functionally mature motor systems of mouse spinal cord. J Physiol. 2012; 590:3821–3839. [PubMed: 22615430]

Bautista W, Nagy JI. Connexin36 in gap junctions forming electrical synapses between motoneurons in sexually dimorphic motor nuclei in spinal cord of rat and mouse. Eur J Neurosci. 2014; 39:771–787. [PubMed: 24304165]

Bautista W, McCrea DA, Nagy JI. Connexin36 identified at morphologically mixed chemical/electrical synapses on trigeminal motoneurons and at primary afferent terminals on spinal cord neurons in adult mouse and rat. Neuroscience. 2014; 263:159–180. [PubMed: 24406437]

Bennett MVL, Pappas G, Gimenez M, Nakajima Y. Physiology and ultrastructure of electrotonic junctions – IV. Medullary electromotor nuclei in gymnotid fish. J Neurophysiol. 1967; 30:236–300. [PubMed: 6045196]

Bennett, MVL. A comparison of electrically and chemically mediated transmission.. In: Pappas, GD.; Purpura, DP., editors. Structure and Function of Synapses. Raven NY: 1972. p. 221-256.

Bennett, MVL. Flexibility and rigidity in electrotonically coupled systems.. In: Bennett, MVL., editor. Synaptic Transmission and Neuronal Interaction. Raven, NY: 1974. p. 153-178.

Bennett, MVL. Electrical transmission: a functional analysis and comparison with chemical transmission.. In: Kandel, ER., editor. Cellular Biology of Neurons, vol I, sec. I, The Handbook of Physiology – The Nervous System I. Williams and Wilkins; Baltimore: 1977. p. 357-416.

Bennett MVL, Goodenough DA. Gap junctions, electrotonic coupling, and intercellular communication. Neurosci Res Pro Bull. 1978; 16:373–485.

Bennett MVL. Gap junctions as electrical synapses. J Neurocytol. 1997; 26:349–366. [PubMed: 9278865]

Bennett MVL, Zukin SR. Electrical coupling and neuronal synchronization in the mammalian brain. Neuron. 2004; 41:495–511. [PubMed: 14980200]

Borst JGG, Helmchen F, Sakmann B. Pre- and postsynaptic whole-cell recordings in the medial nucleus of the trapezoid body of the rat. J Physiol. 1995; 489:825–840. [PubMed: 8788946]

Brazwinsky I, Hartig W, Rubmasen R. Characterization of cochlear nucleus principal cells of Meriones unguiculatus and Monodelphis domestica by use of calcium-binding protein immunolabelling. J Chem Neuroanat. 2008; 35:158–174. [PubMed: 18065198]

Browner RH, Baruch A. The cytoarchitecture of the dorsal cochlear nucleus in the 3-month- and 26-month-old C57BL/6 mouse: a Golgi impregnation study. J Comp Neurol. 1982; 211(2):115–138. [PubMed: 7174885]

Cant NB, Benson CG. Parallel auditory pathways: projection patterns of the different neuronal populations in the dorsal and ventral cochlear nuclei. Brain Res Bull. 2003; 60:457–474. [PubMed: 12787867]

Condorelli DF, Belluardo N, Trovato-Salinaro A, Mudo G. Expression of Cx36 in mammalian neurons. Brain Res Rev. 2000; 32:72–85. [PubMed: 10751658]

Connors BW, Long MA. Electrical synapses in the mammalian brain. Annu Rev Neurosci. 2004; 27:393–418. [PubMed: 15217338]

Connors, BW. Electrical signaling with neuronal gap junctions.. In: Harris, A.; Locke, D., editors. Connexins: A Guide. Humana Press; Springer: 2009. p. 143-164.

Curti S, Hoge G, Nagy JI, Pereda AE. Synergy between electrical coupling and membrane properties promotes strong synchronization of neurons of the mesencephalic trigeminal nucleus. J Neurosci. 2012; 32:4341–4359. [PubMed: 22457486]

Degen J, Meier C, Van der Giessen RS, Sohl G, Petrasch-Parwez E, Urschel S, Dermietzel R, Schilling K, de Zeeuw CI, Willecke K. Expression pattern of lacZ reporter gen representing connexin36 in transgenic mice. J Comp Neurol. 2004; 473:511–525. [PubMed: 15116387]

Devor A, Yarom Y. Electrotonic coupling in the inferior olivary nucleus revealed by simultaeous double patch recordings. J Neurophysiol. 2002; 87:3048–3058. [PubMed: 12037207]

Forsythe ID. Direct patch recording from identified presynaptic terminals mediating glutamatergic EPSCs in the rat CNS, in vitro. J Physiol. 1994; 479:381–387. [PubMed: 7837096]

Friauf E. Distribution of calcium-binding protein calbindin-D28k in the auditory system of adult and developing rats. J Comp Neurol. 1994; 349:193–211. [PubMed: 7860778]

Gibson JR, Beier M, Connors BW. Two networks of electrically coupled inhibitory neurons in neocortex. Nature. 1999; 402:75–79. [PubMed: 10573419]

Gómez-Nieto R, Rubio ME. A bushy cell network in the rat ventral cochlear nucleus. J Comp Neurol. 2009; 516:241–263. PMCID: PMC2841288. [PubMed: 19634178]

Gómez-Nieto R, Rubio ME. Ultrastructure, synaptic organization, and molecular components of bushy cell networks in the anteroventral cochlear nucleus of the rhesus monkey. Neuroscience. 2011; 179:188–207. PMCID: PMC3059371. [PubMed: 21284951]

Goodenough DA, Paul DL. Gap junctions Cold Spring Harb Perspect Biol. 2009; 1:a002576. [PubMed: 20066080]

Herve J-C, Derangeon M. Gap junction mediated cell-to-cell communication. Cell Tiss Res. 2013; 352:21–31.

Hidaka S, Akahori Y, Kurosawa Y. Dendrodendritic electrical synapses between mammalian retinal ganglion cells. J Neurosci. 2004; 24:10553–10567. [PubMed: 15548670]

Hoge GJ, Davidson KGV, Yasumura T, Castillo PE, Rash JE, Pereda AE. The extent and strength of electrical coupling between inferior olivary neurons is heterogeneous. J Neurophysiol. 2011; 105:1089–1101. [PubMed: 21177999]

Hormuzdi SG, Filippov MA, Mitropoulon G, Monyer H, Bruzzone R. Electrical synapses: a dynamic signaling system that shapes the activity of neuronal networks. Biochem Biophys Acta. 2004; 1662:113–137. [PubMed: 15033583]

Horowitz SS, Stamper SA, Simmons JA. Neuronal connexin expression in the cochlear nucleus of big brown bats. Brain Res. 2008:76–84. [PubMed: 18241843]

Joris PX, Smith PH. The volley theory and the spherical cell puzzle. Neuroscience. 2008; 154:65–76. [PubMed: 18424004]

Joris PX, Carney LH, Smith PH, Yin TC. Enhancement of neural synchronization in the anteroventral cochlear nucleus. I. Responses to tones at the characteristic frequency. J Neurophysiol. 1994a; 71:1022–1036. [PubMed: 8201399]

Joris PX, Smith PH, Yin TC. Enhancement of neural synchronization in the anteroventral cochlear nucleus. II. Responses in the tuning curve tail. J Neurophysiol. 1994b; 71:1037–1051. [PubMed: 8201400]

Korn H, Sotelo C, Crepel F. Electrotonic coupling between neurons in the lateral vestibular nucleus. Exp Brain Res. 1973; 16:255–275. [PubMed: 4346867]

Korn H, Sotelo C, Bennett MVL. The lateral vestibular nucleus of the toadfish opsanus Tau: ultrastructural and electrophysiological observations with special reference to electrotonic transmission. Neuroscience. 1977; 2:851–884.

Kriebel ME, Bennett MVL, Waxman SG, Pappas GD. Oculomotor neurons in fish: electrotonic coupling and multiple sites of impulse initiation. Science. 1969; 166:520–524. [PubMed: 4309628]

Leznik E, Llinas R. Role of gap junctions in synchronized neuronal oscillations n the inferor olive. J Neurophysiol. 2005; 94:2447–2456. [PubMed: 15928056]

Li X, Kamasawa N, Ciolofan C, Olson CO, Lu S, Davidson KGV, Yasumura T, Shigemoto R, Rash JE, Nagy JI. Connexin45-containing neuronal gap junctions in rodent retina also contain connexin36 in both apposing hemiplaques, forming bi-homotypic gap junctions, with scaffolding contributed by zonula occludens-1. J Neurosci. 2008; 28:9769–89. [PubMed: 18815262]

Loftus WC, Malmierca MS, Bishop DC, Oliver DL. The cytoarchitecture of the inferior colliculus revisited: a common organization of the lateral cortex in rat and cat. Neuroscience. 2008; 154:196–205. [PubMed: 18313229]

Logan SD, Pickering AE, Gibson IC, Nolan MF, Spanswick D. Electrotonic coupling between rat sympathetic preganglionic neurones in vitro. J Physiol. 1996a; 495:491–502. [PubMed: 8887759]

Logan SD, Spanswick D, Pickering AE, Gibson IC, Cammack NC. Gap junction coupling and the regulation of excitability in sympathetic preganglionic neurons. J Aut Ner Syst. 1996b; 58:202–226.

Mann-Metzer P, Yarom Y. Electrotonic coupling interacts with intrinsic properties to generate synchronized activity in cerebellar networks of inhibitory interneurons. J Neurosci. 1999; 19:3298–3306. [PubMed: 10212289]

Martin EM, Devidze N, Shelley DN, Westberg L, Fontaine C, Pfaff DW. Molecular and neuroanatomical characterization of single neurons in the mouse medullary gigantocellular reticular nucleus. J Comp Neurol. 2011; 519:2574–2593. [PubMed: 21456014]

Meier C, Dermietzel R. Electrical synapses--gap junctions in the brain. Results Probl Cell Differ. 2006; 43:99–128. [PubMed: 17068969]

Merchan MA, Collia F, Lopez DE, Saldana E. Morphology of cochlear root neurons in rat. J Neurocytol. 1988; 17:711–725. JA. [PubMed: 2463341]

Mugnaini E. GABA neurons in the superficial layers of the rat dorsal cochlear nuclues: light and electron microscopic immunocytochemistry. J Comp Neurol. 1985; 235:61–81. [PubMed: 3886718]

Nagy JI. Evidence for connexin36 localization at hippocampal mossy fiber terminals suggesting mixed chemical/electrical transmission by granule cells. Brain Res. 2012; 1487:107–122. [PubMed: 22771400]

Nagy JI, Bautista W, Blakley B. Morphologically mixed chemical-electrical synapses in developing and adult rodent vestibular nuclei as revealed by immunofluorescence detection of connexin36 and vesicular glutamate transporter-1. Neuroscience. 2013; 252:468–488. [PubMed: 23912039]

Nagy JI, Urena-Ramirez V, Ghia J-E. Functional alterations in gut contractility after connexin36 ablation and evidence for gap junctions forming electrical synapses between nitrergic enteric neurons. FEBS Letts. 2014; 588:1480–90. [PubMed: 24548563]

Palacios-Prado N, Chapuis S, Panjkovich A, Freqeac J, Nagy JI, Bukauskas FF. Molecular determinants of magnesium-dependent synaptic plasticity at electrical synapses formed by connexin36. Nature Comm. 2014; 5:4667–4680.

Paolini AG, FitzGerald JV, Burkitt AN, Clark GM. Temporal processing from the auditory nerve to the medial nucleus of the trapezoid body in the rat. Hear Res. 2001; 159:101–116. [PubMed: 11520638]

Pappas GD, Bennett MVL. Specialized junctions involved in electrical transmission between neurons. Ann NY Acad Sci. 1966; 137:495–508. [PubMed: 5229811]

Pereda A, O'Brien J, Nagy JI, Bukauskas F, Davidson KGV, Yasumura T, Rash JE. Connexin35 mediates electrical transmission at mixed synapses on Mauthner cells. J Neurosci. 2003; 23:7489–7503. [PubMed: 12930787]

Pereda A, Rash JE, Nagy JI, Bennett MVL. Dynamics of electrical transmission at club endings on the Mauthner cells. Brain Res Rev. 2004; 47:227–244. [PubMed: 15572174]

Pereda AE, Curti S, Hoge G, Cachope R, Flores CE, Rash JE. Gap junction-mediated electrical transmission: Regulatory mechanisms and plasticity. Biochim Biophys Acta. 2013; 1828:134–146. [PubMed: 22659675]

Pereda AE. Electrical synapses and their functional interactions with chemical synapses. Nat Rev Neurosci. 2014; 15:250–263. [PubMed: 24619342]

Rash JE, Dillman RK, Bilhartz BL, Duffy H S, Whalen L R, Yasumura T. Mixed synapses discovered and mapped throughout mammalian spinal cord. Proc Natl Acad Sci (USA). 1996; 93:4235–4239. [PubMed: 8633047]

Rash JE, Staines WA, Yasumura T, Pate D, Hudson CS, Stelmack GL, Nagy J. Immunogold evidence that neuronal gap junctions in adult rat brain and spinal cord contain connexin36 (Cx36) but not Cx32 or Cx43. Proc Natl Acad Sci (USA). 2000; 97:7573–7578. [PubMed: 10861019]

Rash JE, Yasumura T, Dudek FE, Nagy JI. Cell-specific expression of connexins, and evidence for restricted gap junctional coupling between glial cells and between neurons. J Neurosci. 2001; 21:1983–2000. [PubMed: 11245683]

Rash JE, Pereda A, Kamasawa N, Furman CS, Yasumura T, Davidson KGV, Dudek FE, Olson C, L X, Nagy JI. High-resolution proeomic mapping in the vertebrate central nervous system: Close proximity of connexin35 to NMDA glutamate receptor clusters and co-localization of connexin36 with immunoreactivity for zonula occludens protein-1 (ZO-1). J Neurocytol. 2004; 33:131–151. [PubMed: 15173637]

Rash JE, Davidson KGV, Kamasawa N, Yasumura T, Kamasawa M, Zhang C, Michaels R, Restrepo D, Ottersen OP, Olson C, Nagy JI. Ultrastructural localization of connexins (Cx36, Cx43, Cx45), glutamate receptors and aquaporin-4 in rodent olfactory mucosa, olfactory nerve and olfactory bulb. J Neurocytol. 2005; 34:309–342.

Rash JE, Olson CO, Pouliot WA, Davidson KGV, Yasumura T, Furman CS, Royer S, Kamasawa N, Nagy JI, Dudek FE. Connexin36, miniature neuronal gap junctions, and limited electrotonic coupling in rodent suprachiasmatic nucleus (SCN). Neuroscience. 2007a; 149:350–371. [PubMed: 17904757]

Rash JE, Olson CO, Davidson KGV, Yasumura T, Kamasawa N, Nagy JI. Identification of connexin36 in gap junctions between neurons in rodent locus coeruleus. Neuroscience. 2007b; 147:938–956. [PubMed: 17601673]

Rash JE, Curti S, Vanderpool KG, Kamasawa N, Nannapaneni S, Palacios-Prado N, Flores CE, Yasumura T, O'Brien J, Lynn BD, Bukauskas FF, Nagy JI, Pereda AE. Molecular and functional asymmetry at a vertebrate electrical synapse. Neuron. 2013; 79:957–969. [PubMed: 24012008]

Rash JE, Kamasawa N, Vanderpool KG, Yasumura T, O'Brien J, Nannapaneni S, Pereda A, Nagy JI. Heterotypic gap junctions at glutamatergic mixed synapses are abundant in goldfish brain. Neuroscience. 2014; 285:166–193. [PubMed: 25451276]

Rollenhagen A, Lubke JHR. The morphology of excitatory central synapses: From structure to function. Exp Tiss Res. 2006; 326:221–237.

Rubio ME, Gudsnuk KA, Smith Y, Ryugo DK. Revealing the molecular layer of the primate dorsal cochlear nucleus. Neuroscience. 2008; 154:99–113. [PubMed: 18222048]

Schofield BR, Cant NB. Organization of the superior olivary complex in the guinea pig: II. Patterns of projection from the periolivary nuclei to the inferior colliculus. J Comp Neurol. 1992; 317:438–455. [PubMed: 1578006]

Söhl G, Maxeiner S, Willecke K. Expression and functions of neuronal gap junctions. Nat Rev Neurosci. 2005; 6:191–200. [PubMed: 15738956]

Sotelo, C. Morphological correlates of electrotonic coupling between neurons in mammalian nervous system.. In: Santini, M., editor. Golgi Centennial Symposium. Raven Press; New York: 1975. p. 355-365.

Sotelo C, Gentschev T, Zamora AJ. Gap junctions in the ventral cochlear nucleus of the rat. A possible new example of electrotonic junctions in the mammalian CNS. Neuroscience. 1976; 1:5–7. [PubMed: 980250]

Sotelo C, Korn H. Morphological correlates of electrical and other interactions through low-resistance pathways between neurons of the vertebrate central nervous system. Int Rev Cytol. 1978; 5:67–107. [PubMed: 389866]

Sotelo, C.; Triller, A. Morphological correlates of electrical, chemical and dual modes of transmission.. In: Stjarne, L.; Lagercrantz, L.; Hedqvist, H.; Wennmalm, A., editors. Chemical neurotransmission, 75 years. Academic Press; New York: 1982. p. 13-28.

Thompson AM, Schofield BR. Afferent projections of the superior olivary complex. Micros Res Tech. 2000; 51:330–354.

Trettel, J.; Morest, DK. The Handbook of Mouse Auditory Research. CRC Press LLC; 2001. Cytoartichectonic atlas of the cochlear nucleus of the mouse.; p. 279-296.

Vivar C, Traub RD, Gutierrez R. Mixed electrical–chemical transmission between hippocampal mossy fibers and pyramidal cells. Eur J Neurosci. 2012; 35:76–82. [PubMed: 22151275]

Wellershaus K, Degen J, Deuchars J, Theis M, Charollais A, Caille D, Gauthier B, Janssen-Bienhold U, Sonntag S, Herrera P, Meda P, Willecke K. A new conditional mouse mutant reveals specific expression and functions of connexin36 in neurons and pancreatic beta-cells. Exp Cell Res. 2008; 314:9971012.

Wouterlood FG, Mugnaini E, Osen KK, Dahl A-L. Stellate neruons in rat dorsal cochlear nucleus studied with combined Golgi impregnation and electron microscopy: synaptic connections and mutual coupling by gap junctions. J Neurocytol. 1984; 13:639–664. [PubMed: 6481413]

Wylie RM. Evidence of electrotonic transmission in the vestibular nuclei of the rat. Brain Res. 1973; 50:179–183. [PubMed: 4347844]

Zhou J, Nannapaneni N, Shore S. Vesicular glutamate transporters 1 and 2 are differentially associated with auditory nerve and spinal trigeminal inputs to the cochlear nucleus. J Comp Neurol. 2007; 500:777–787. [PubMed: 17154258]

Highlights

- Cx36 is widely expressed in the auditory system of rat and mouse
- Neuronal gap junctions composed of Cx36 are abundant in the auditory system
- Auditory nuclei contain nerve terminals forming morphologically mixed synapses
- Nerve terminals associated with Cx36 in the cochlear nucleus are of primary afferent origin

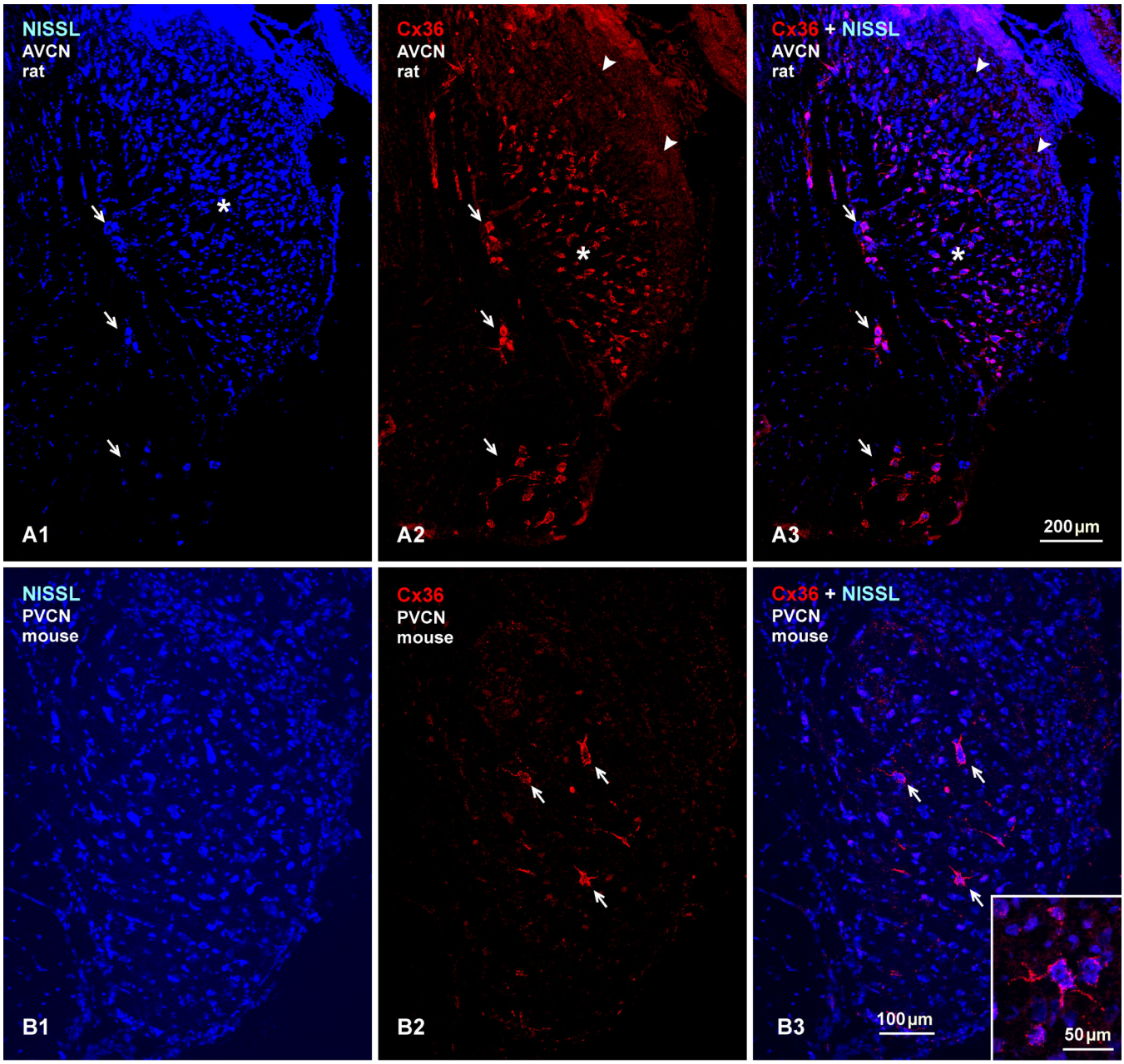

Fig. 1.

Low magnification overview of immunofluorescence labelling for Cx36 with blue Nissl counterstain in the AVCN and PVCN of adult rat and mouse. (A1-A3) Image of the AVCN at the level of the auditory nerve entry root, showing neurons distributed throughout the main part of the nucleus (A1, asterisk) as well as dispersed neurons located in the 8th nerve entry zone (A1, arrows). Image of the same field shows immunolabelling for Cx36 (A2), which is prominent in the ventromedial portion of the AVCN (A2, asterisk) and in the 8th nerve root entry zone (A2, arrows). In both regions, Cx36 is localized to the majority of neuronal cell bodies, as shown by blue/red overlay (A3, asterisk and arrows). The dorsolateral portion of the AVCN contains only sparse labelling for Cx36 (A2, arrowheads).

(B1-B3) Image of the PVCN at a posterior level of adult mouse, showing neurons in all parts of the nucleus (B1), but heavy labelling of Cx36 associated only with what appear to be octopus cells (B2, B3 arrows), with a higher magnification of a Cx36-positive octopus cell shown in the inset.

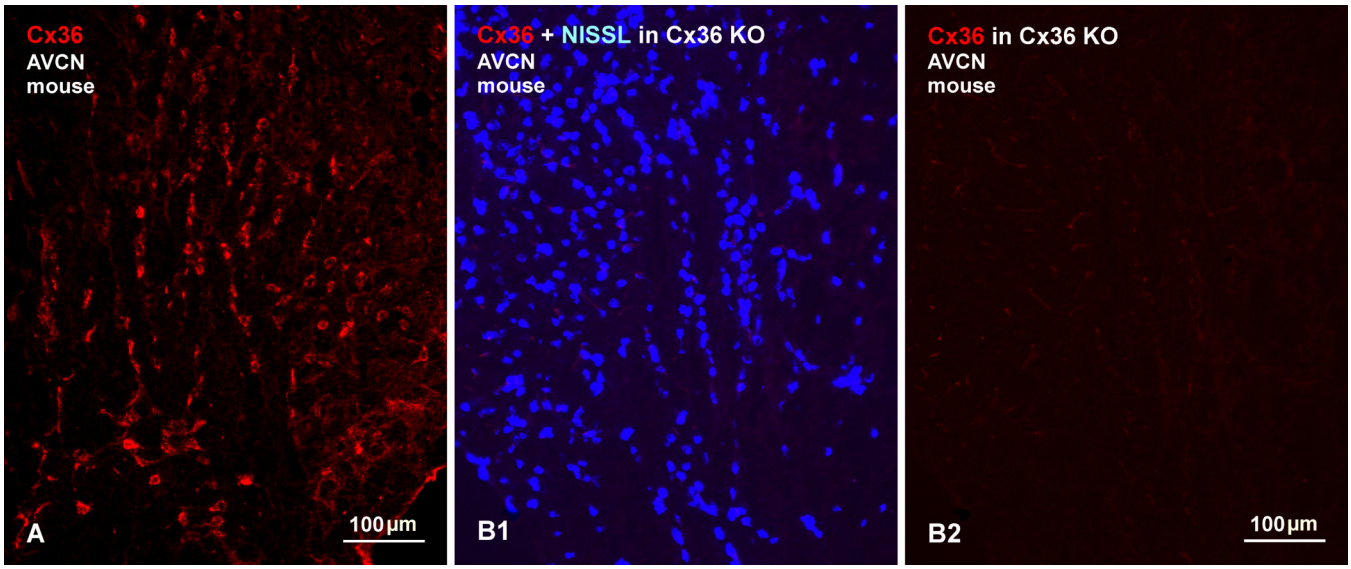

Fig. 2.

Immunofluorescence of Cx36 in the AVCN of mouse. (A) The central region of the AVCN from a wild-type mouse brain, showing similar labelling for Cx36 as seen in rat. (B) Images of a field in the AVCN corresponding to that in (A), but from a Cx36 knockout mouse, showing numerous Nissl stained neurons in the field (B1) and an absence of labelling for Cx36 in the same field (B2).

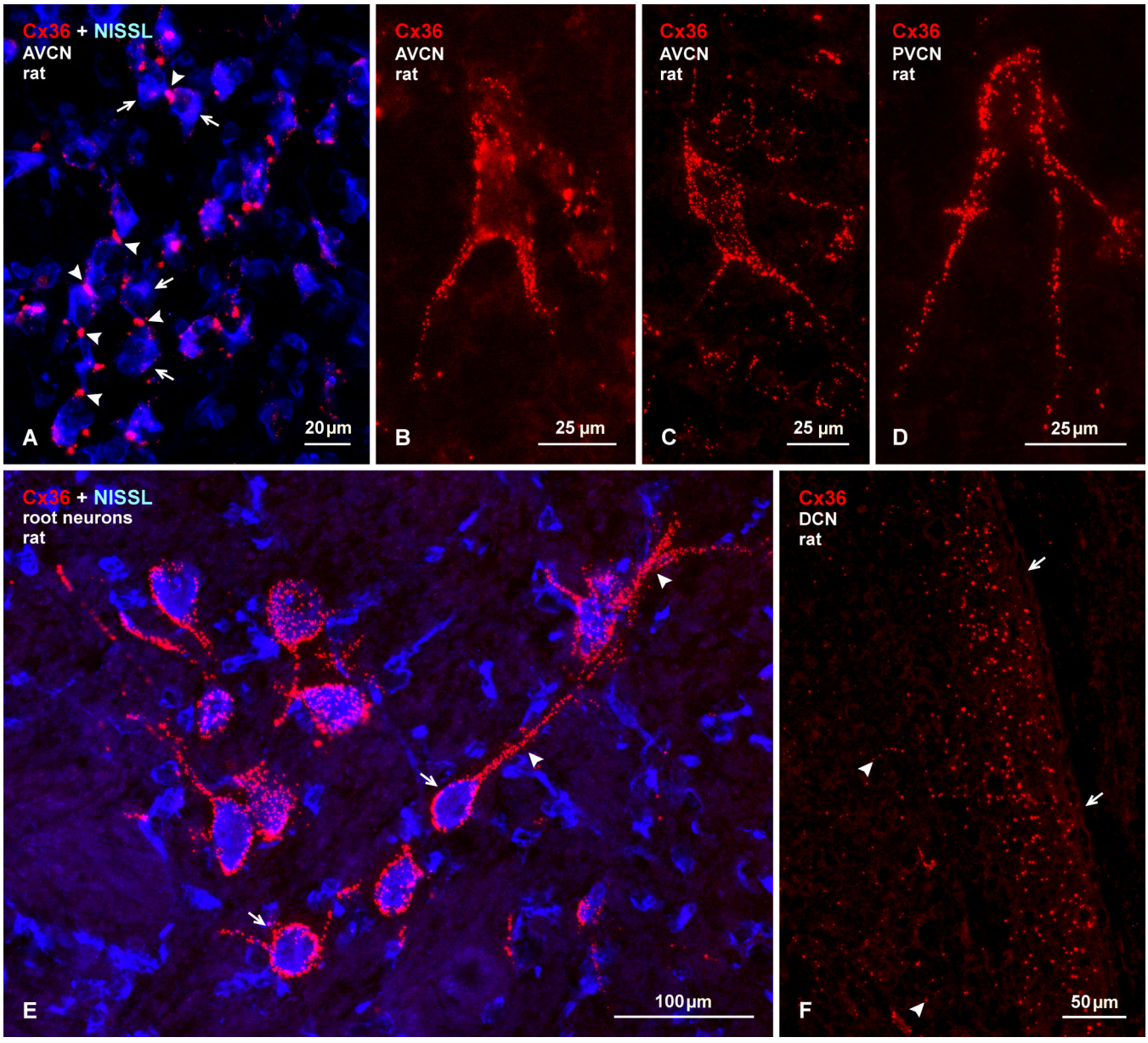

Fig. 3.

Patterns of immunofluorescence labelling for Cx36 in the cochlear nuclei of adult rat. (A) Image shows Cx36 labelling with blue Nissl counterstain in the AVCN. Cx36-puncta (arrowheads) are seen at neuronal somatic appositions linking multiple neurons (arrows) in sequence. (B-D) Images showing Cx36-puncta distributed on cell bodies and initial dendrites of large multipolar neurons in the AVCN (B, C) and octopus neurons in the PVCN (D). (E) Image with blue Nissl counterstaining shows a cluster of auditory root neurons with numerous Cx36-puncta on neuronal somata (arrows) and along dendrites (arrowheads). Labelling of Cx36 is exclusively punctate, and is localized on neuronal surfaces with negligible intracellular labelling. (F) Immunolabelling of Cx36 in the DCN, showing a moderate density of Cx36-puncta scattered in the superficial molecular layer (arrows), and sparsely distributed Cx36-puncta in deeper layers (arrowheads).

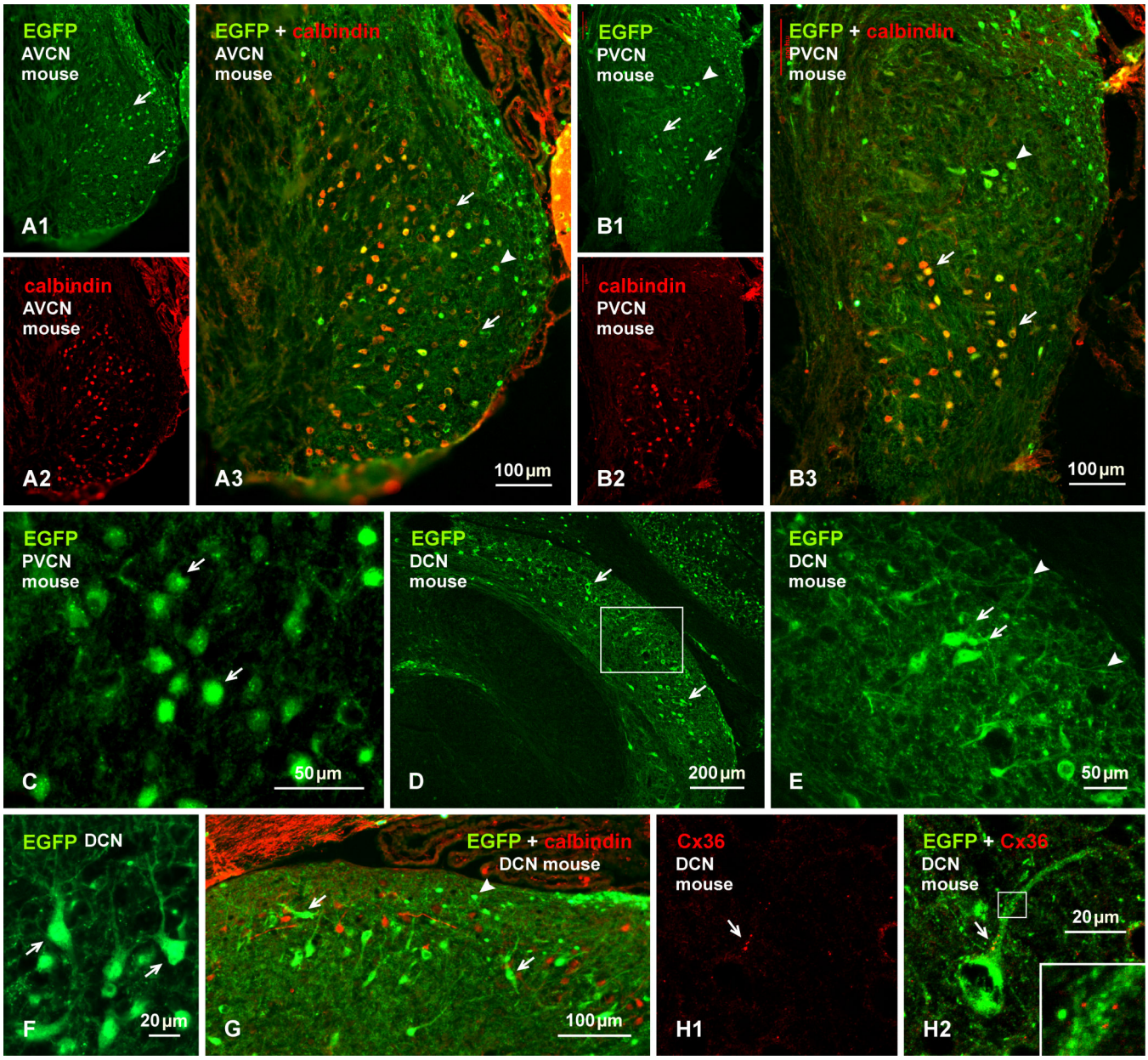

Fig. 4.

Immunofluorescence labelling of EGFP in combination with calbindin or Cx36 in adult EGFP-Cx36 mice. (A, B) The AVCN showing labelling for EGFP (A1) and calbindin (A2) in the same field and with overlay (A3) in an anterior region of the nucleus, and labelling for EGFP (B2) and calbindin (B2) in the same field and with overlay (B3) in the PVCN. EGFP-positive neurons are distributed in the AVCN (A1, arrows), and in the PVCN (B1), and many in both regions are calbindin-positive (A3,B3, arrows), but some in the dorsal PVCN are devoid of calbindin (B1, B3, arrowheads). (C) Labelling for EGFP is localized mainly to neuronal somata, including cellular nuclei (arrows). (D, E) Labelling for EGFP in the DCN, with the boxed area in (D) shown at higher magnification in (E). EGFP-positive neurons are seen throughout the nucleus, but are most concentrated near the border between the fusiform

cell and molecular layer (D, arrow), with labelling in soma (E, arrows) and less so in dendritic processes (E, arrowheads). (F) Higher magnification of EGFP-positive neurons (arrows) in the fusiform cell layer with dendrites directed towards the molecular layer. (G) The DCN with immunolabelling of EGFP in combination with calbindin. Both large EGFP-positive cells in superficial regions of the fusiform cell layer (arrows) and small EGFP-positive cells in the molecular layer (arrowheads) are devoid of labelling for calbindin. (H) Immunolabelling of EGFP and Cx36 in the same field at the border between the fusiform and molecular layer, showing Cx36-puncta (H1, arrow) localized to the initial dendritic segment of an EGFP-positive neuron, as seen in overlay (H2, arrow) and at higher magnification (H2, inset).

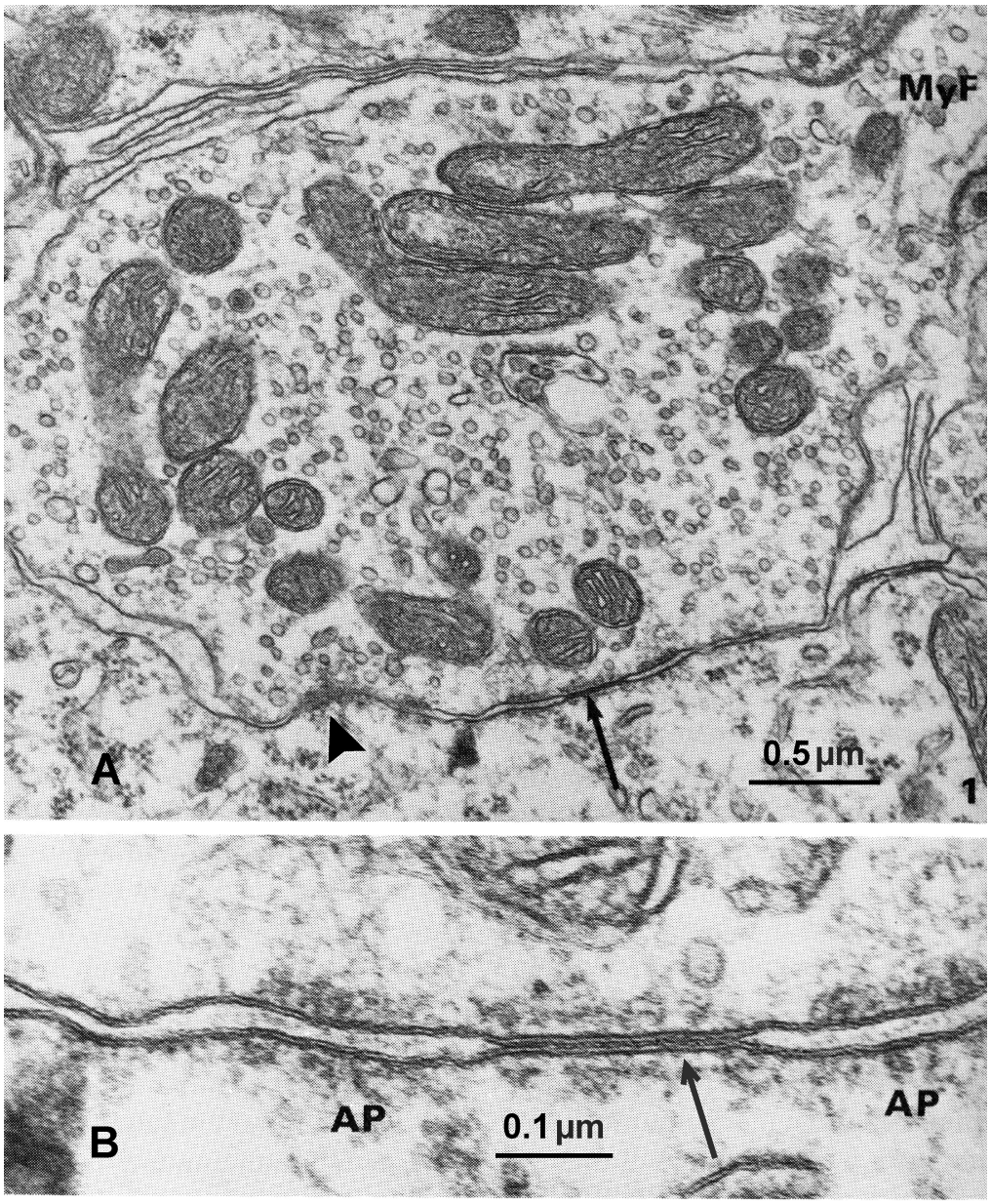

Fig. 5.

Reproduced from Sotelo and Triller (1982), with permission from Global Rights Dept, Elsevier (scale bars added). (A, B) Electron micrograph of a large axon terminal contacting a postsynaptic neuron in the ventral cochlear nucleus in adult rat. The terminal displays numerous clear and round synaptic vesicles and forms a gap junction with the postsynaptic neuron (A, arrow), which is shown at higher magnification in (B, arrow). Also seen are attachment plaques (AP) (aka, adherens junction) at each side of the gap junction, and a postsynaptic density at a site of vesicle accumulation (arrowhead).

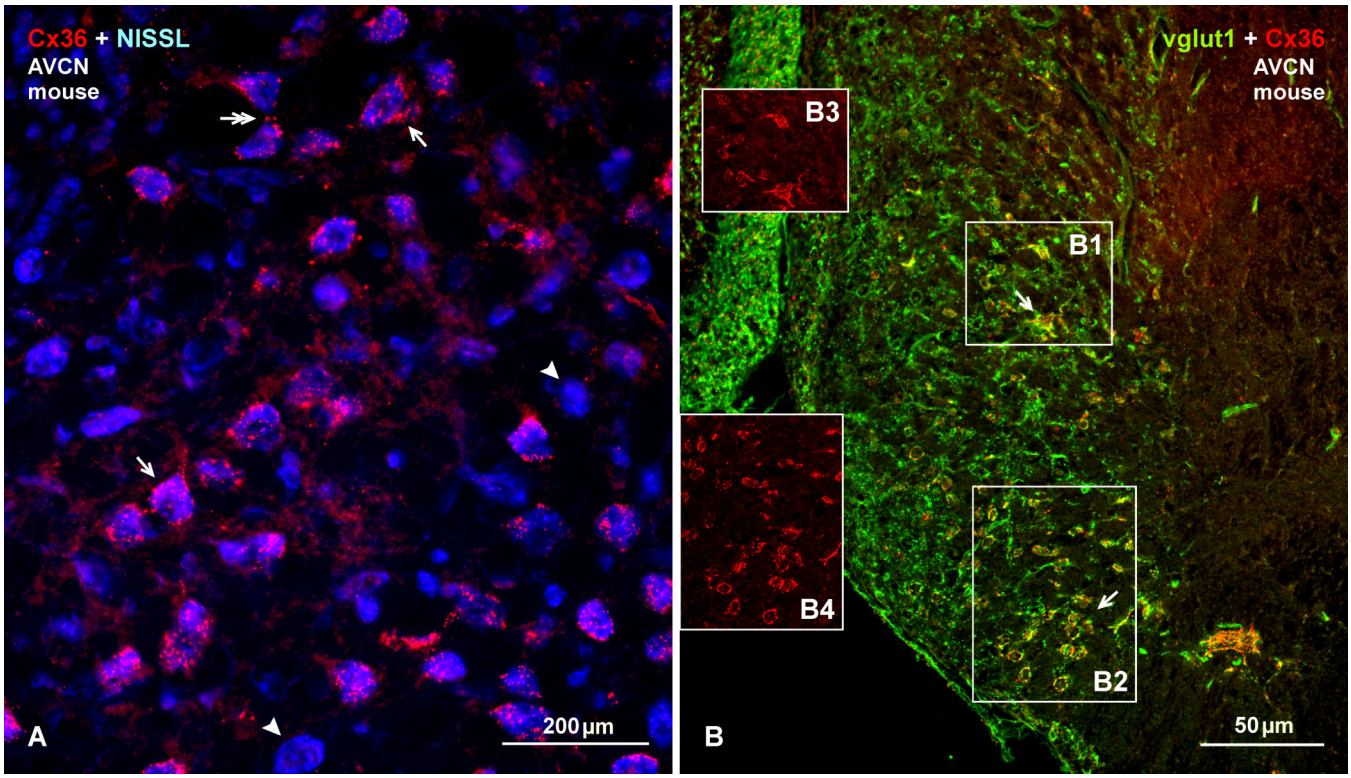

Fig. 6.

Immunofluorescence of Cx36 in adult mouse AVCN and co-distribution with vglut1. (A) Image with blue Nissl counterstaining shows similar patterns of immunolabelling for Cx36 in the AVCN of mouse as observed in the AVCN of rat. Abundant Cx36-puncta are seen around many (arrows) but not all (arrowheads) neuronal cell bodies, and some puncta occur at neuronal appositions (double arrow). (B) Image of double-labelling for Cx36 (red) and vglut1 (green), showing a high density of labelling for vglut1 around most neuronal somata in the AVCN, and its co-localization with Cx36 (seen as yellow at sites of red/green overlap) at a subpopulation of these neurons (arrows). Boxed areas (B1, B2) are shown in insets with labelling for Cx36 alone (B3, B4, respectively).

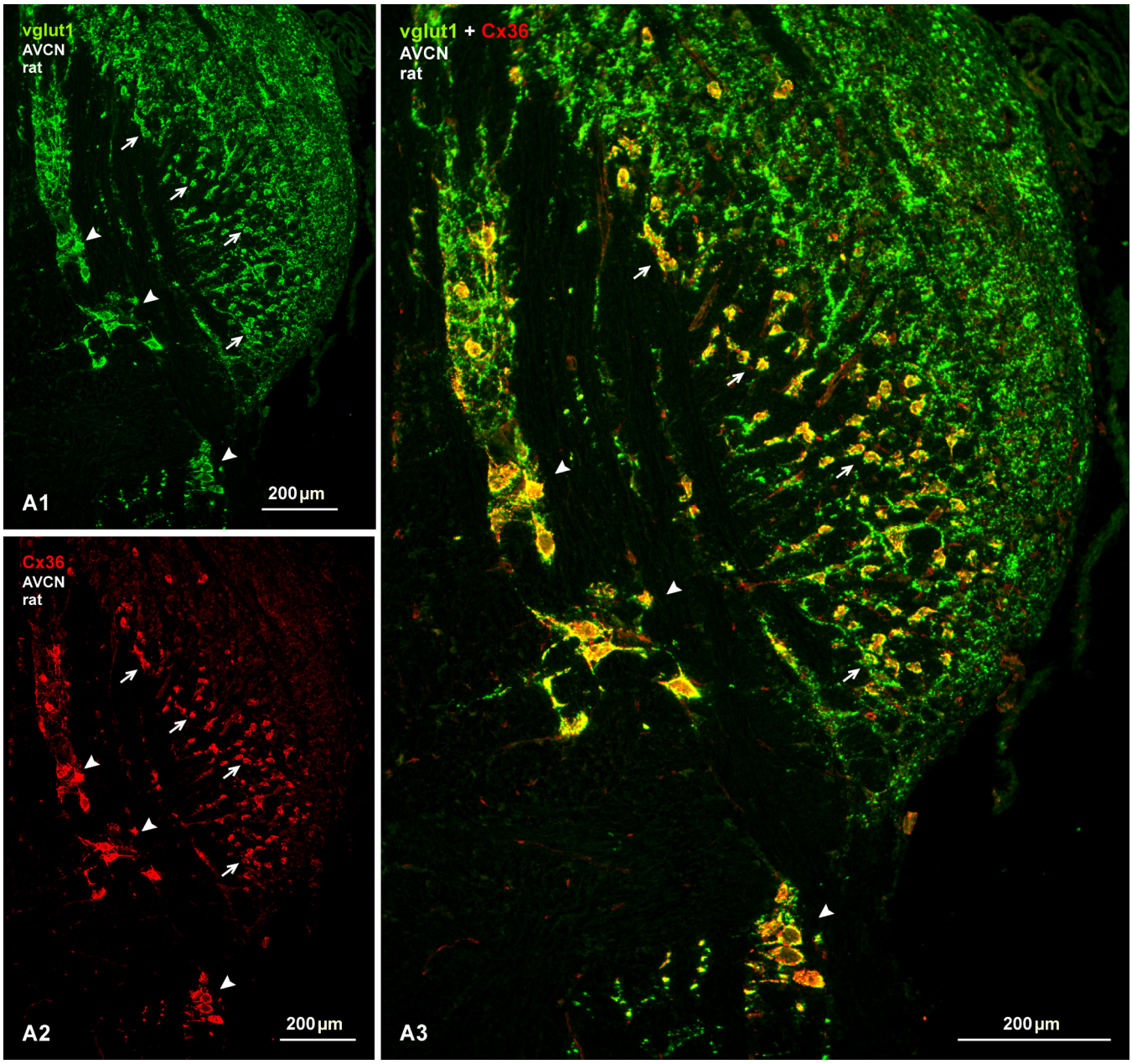

Fig. 7.

Double immunofluorescence labelling of vglut1 and Cx36 in the AVCN of adult rat. (A) low magnification wide-field images showing labelling for vglut1 (A1) alone and, in the same field, labelling for Cx36 alone (A2), and after image overlay (A3). Terminals labelled for vglut1 are distributed throughout the AVCN, and are heavily concentrated on large ventrally located neurons in the nucleus (arrows) and on large auditory root neurons along their dorso-ventral extension along the 8th nerve entry zone (arrowheads). Terminals positive for vglut1 on these neurons are localized largely to neuronal somata and only rarely along initial dendritic processes. Dense labelling of Cx36 is seen on neurons that are richly covered with

vglut1-postive terminals, as seen by yellow after green/red overlay (A3, arrows and arrowheads).

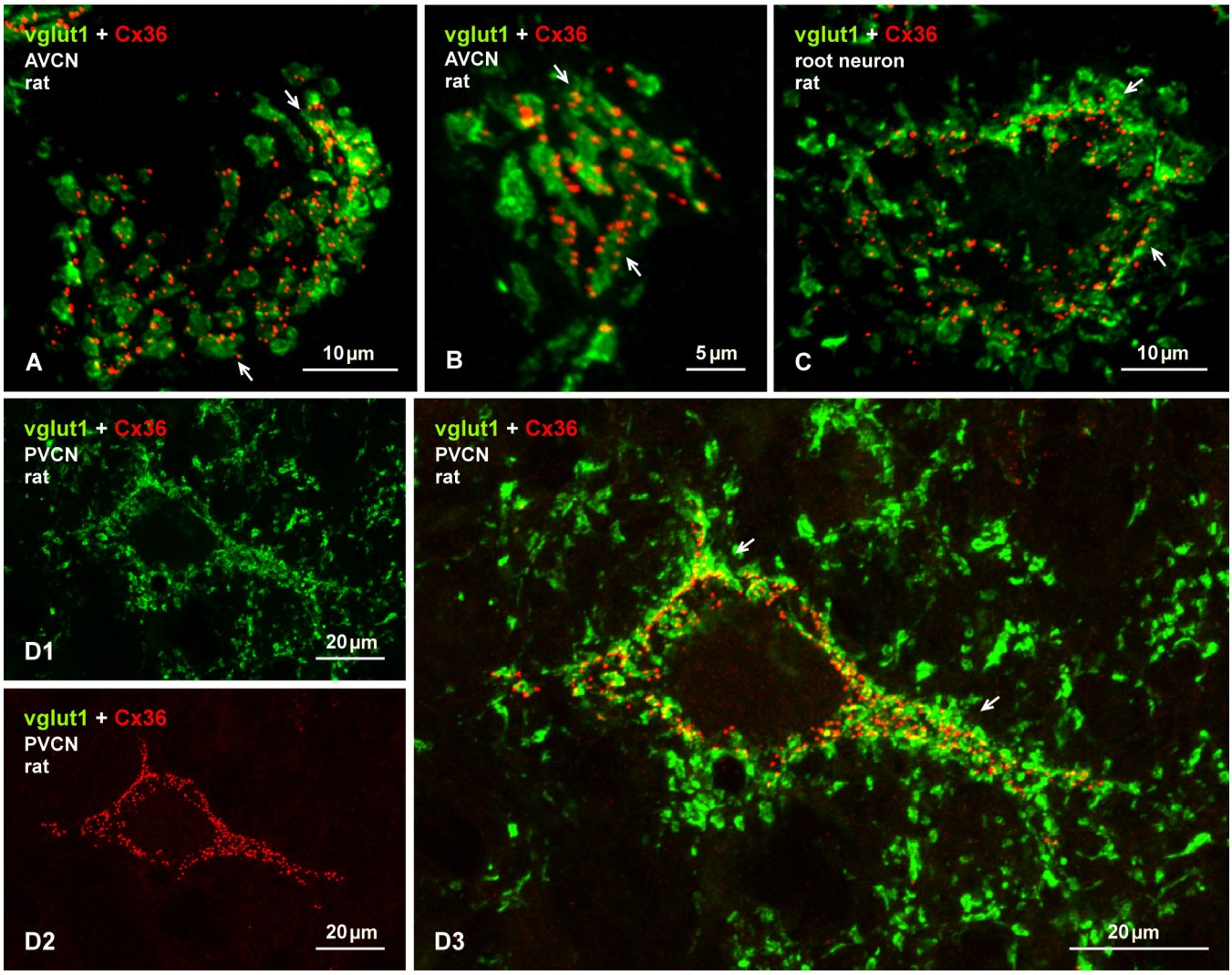

Fig. 8.

Laser scanning confocal double immunofluorescence of Cx36 and vglut1 in the AVCN and PVCN of adult rat. (A-C) Image overlays of labelling for Cx36 (red) and vglut1 (green) in association with neuronal somata in a dorsal (A) and ventral (B) region of the AVCN, and with a neuronal somata of a auditory root neuron (C). In each case, Cx36-puncta are largely localized to regions of labelling for vglut1 on these somata (arrows). (D) Immunolabelling of vglut1 (D1) and in the same field labelling of Cx36 (D2) associated with a large neuron resembling an octopus cell in the PVCN; only a portion of its dendrites were captured in this sections. Densely distributed vglut1-positive terminals and Cx36-puncta around the neuronal soma and its initial dendrites display a high degree of co-localization (D3, arrows, seen as yellow at sites of red/green overlap). Terminals labelled for vglut1 in surrounding regions are devoid of labelling for Cx36.

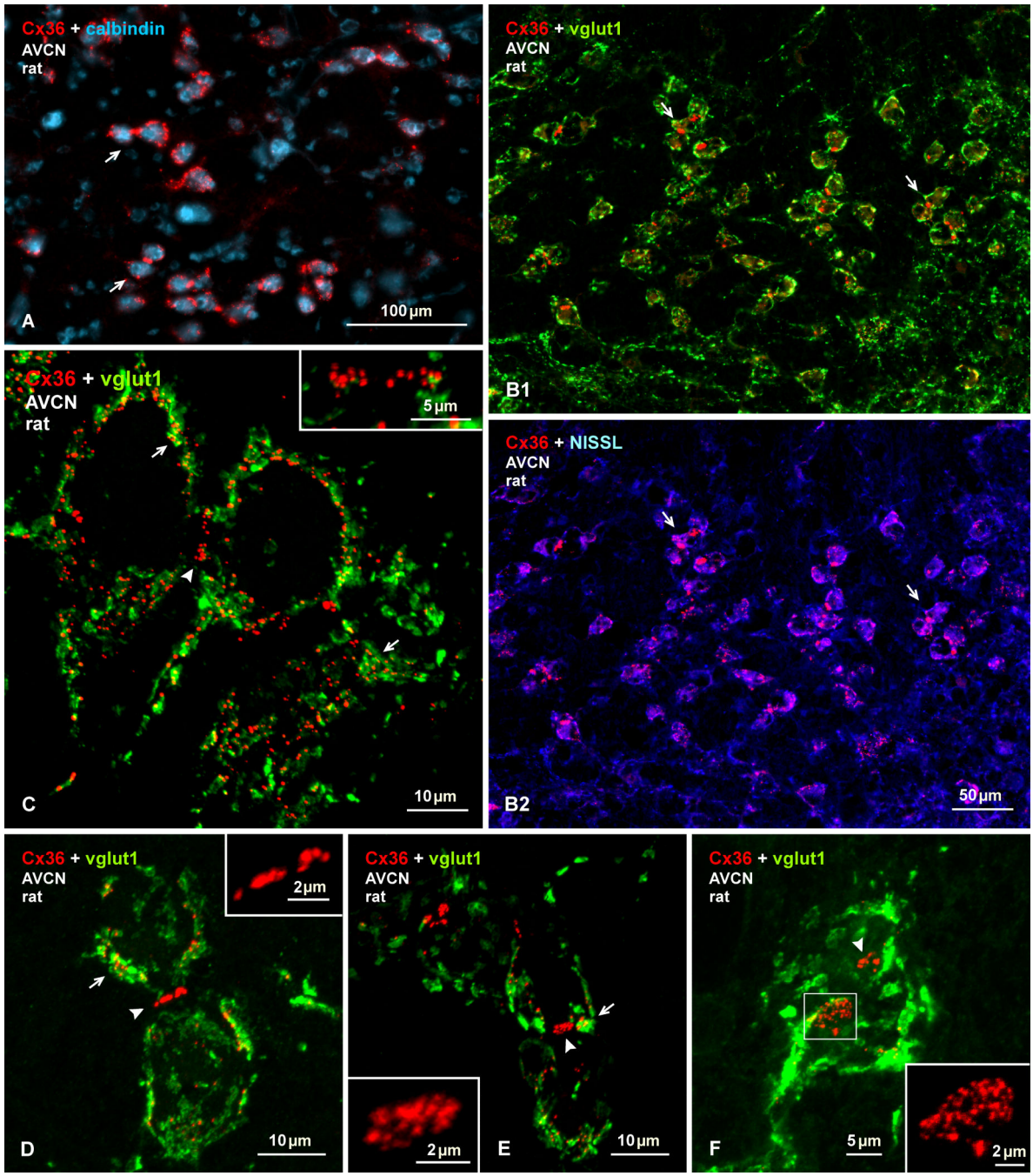

Fig. 9.

Immunolabelling of Cx36 at purely electrical synapses in the AVCN of adult rat. (A) Cx36-puncta are localized around small and medium sized calbindin-positive neurons (labelled blue, arrows). (B) Images of the same field showing dense labelling for vglut1 (green) around neuronal somata displaying Cx36-puncta (red) at their appositions (arrows), as shown with red/green overlay (B1), and as red with blue Nissl counterstain (B2). (C) Cconfocal magnification, showing Cx36/vglut1 co-localization around somata (arrows) and an absence of labelling for vglut1 at somatic appositions displaying Cx36-puncta

(arrowhead). (D-F) Confocal images showing labelling of Cx36 and vglut1, with Cx36 at somatic appositions. Cx36-puncta are visualized as linear arrangements at somatic appositions viewed en edge (D, arrowhead; magnified in inset), or as collections of puncta at appositions viewed at an oblique angle (E, arrowhead; magnified in inset), or as large patches of numerous Cx36-puncta at appositions viewed en face (F, arrowhead, and boxed area shown at higher magnification in inset).

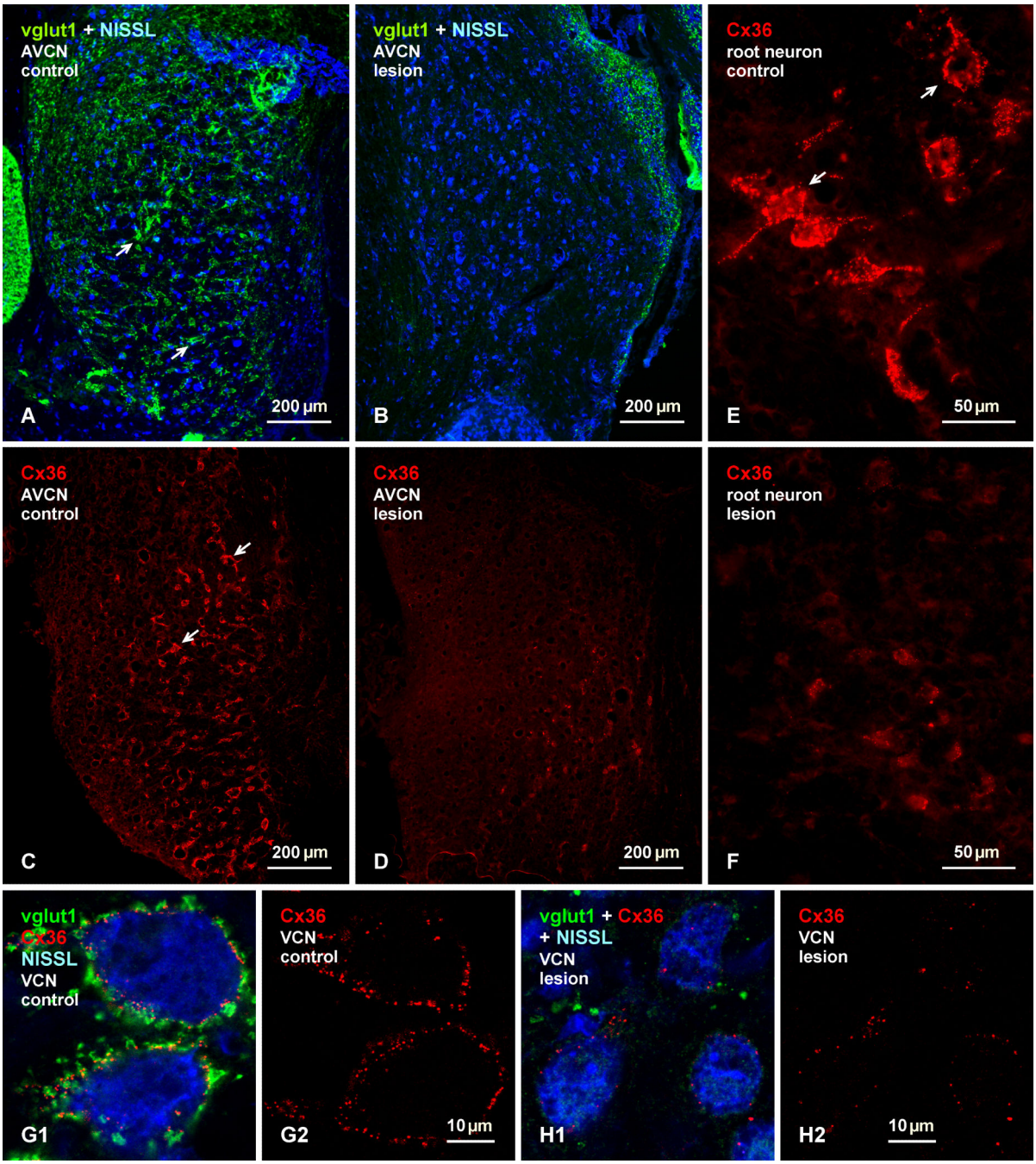

Fig. 10.

Depletion of vglut1 and Cx36 in the AVCN of adult rat after unilateral cochlear ablation. (A, B) Blue Nissl counterstained sections showing the left intact AVCN with its normal complement of dense labelling for vglut1 on neuronal somata and initial dendrites (A, arrows), and the right deafferented AVCN with a near total loss of labelling for vglut1 throughout the nucleus (B). (C, D) Similar field as in (A, B) labelled for Cx36, showing a large number of neurons decorated with Cx36-puncta in the AVCN on the control unlesioned side (C, arrows) and a substantial depletion of labelling for Cx36 in the AVCN

on the deafferented side (D). (E, F) Images showing a normal distribution of Cx36-puncta associated with auditory root neurons in the intact cochlear nucleus (E, arrows), and a depletion of Cx36 on these neurons in the contralateral deafferented cochlear nucleus (F). (G, H) The ventral cochlear nuclei at higher magnification of labelling for vglut1 and Cx36 with Nissl counterstaining (G1) and the same field with labelling for Cx36 only on the control (G) side, and a similar set of images from the lesion (H) side, showing signal confocal scans of areas that were used for counts of Cx36-puncta associated with neuronal somata on each side.

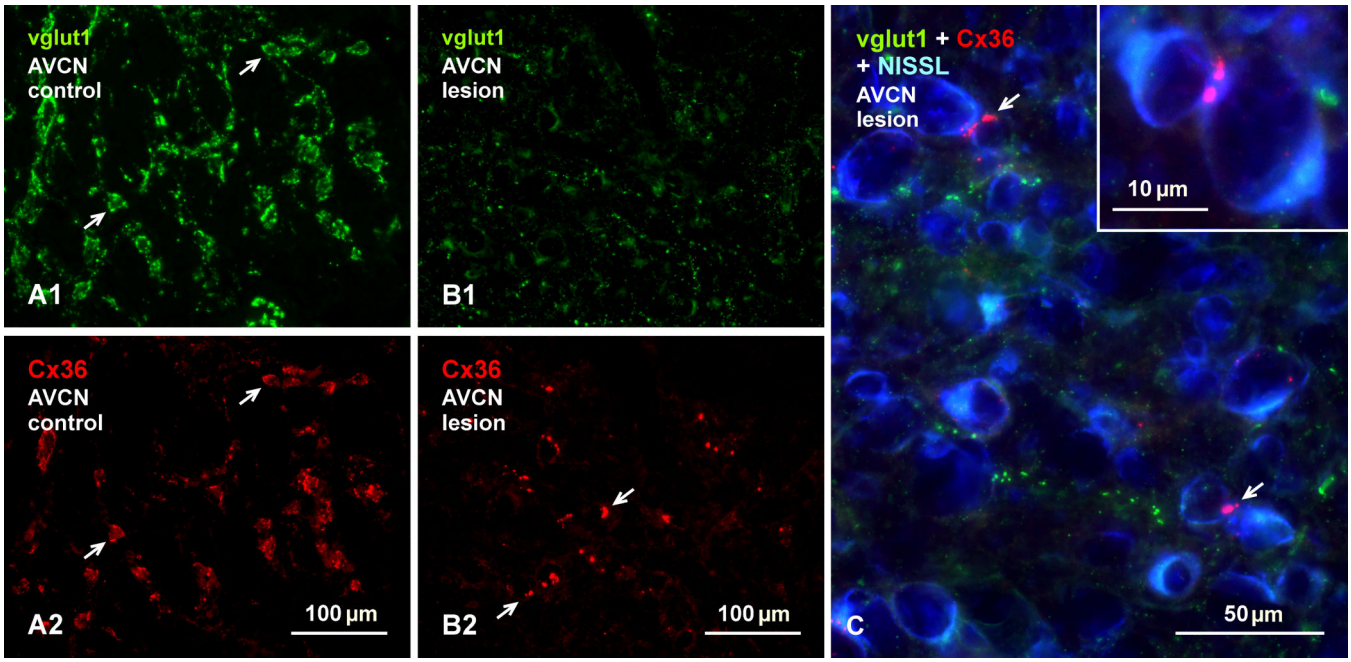

Fig. 11.

Persistence of Cx36 at sites of somatic appositions in the AVCN of adult rat after unilateral cochlear ablation. (A, B) Images of the same field in the intact AVCN (A), showing small and medium sized neuronal somata with their normal labelling for vglut1 (A1, arrows) and Cx36 (A2, arrows), and a similar field in the deafferented AVCN (B1, B2) showing a large loss of vglut1 and Cx36 on these neurons, and a persistence of Cx36-puncta (B2, arrows) localized at appositions between neuronal somata. (C) Higher magnification of a field similar to that in (B) on the lesioned side counterstained with blue Nissl, showing a large loss of labelling for vglut1 around neuronal somata, and an absence of labelling for Cx36 around these somata except at points of their appositions (arrows), shown magnified in the inset.

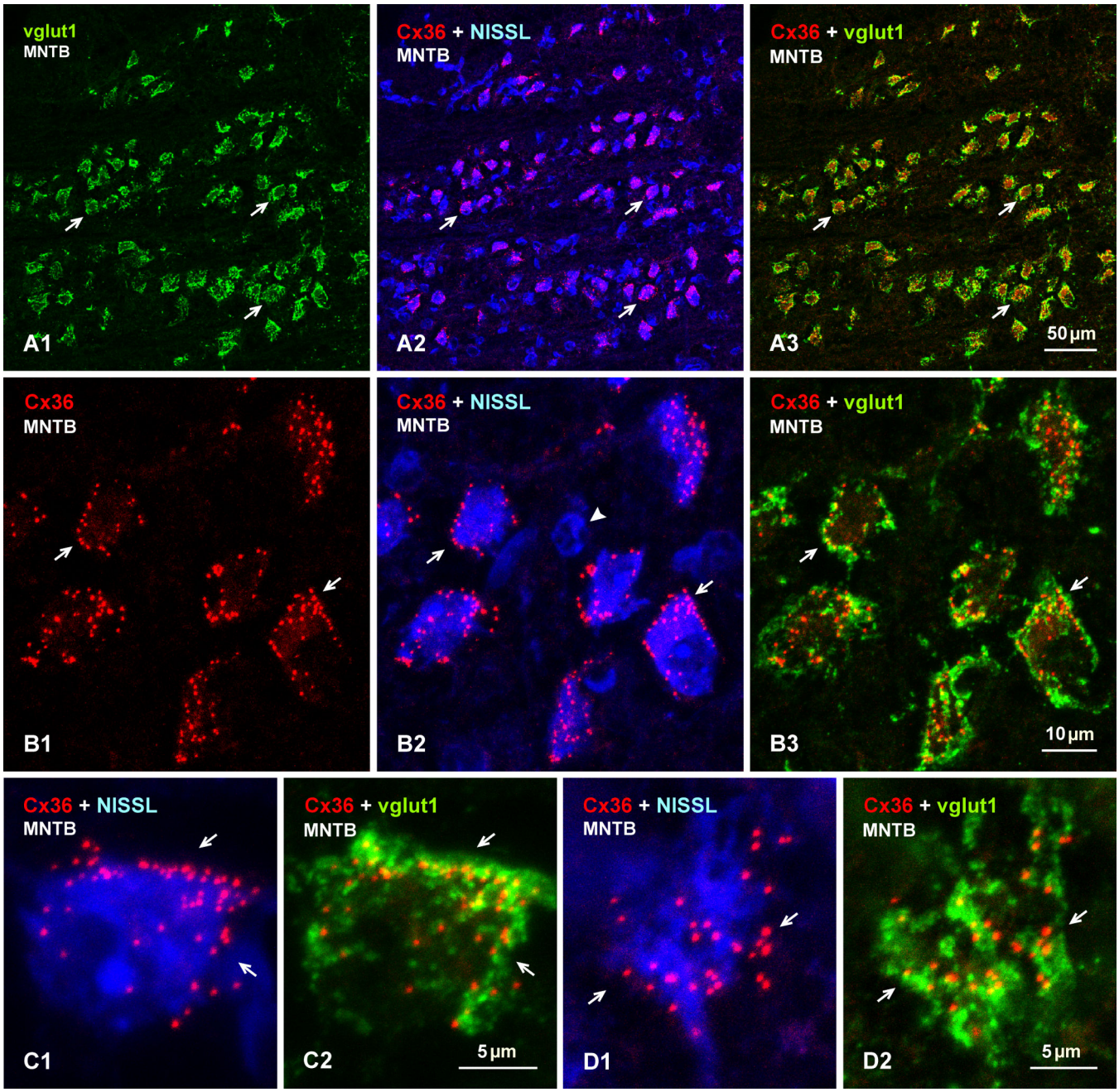

Fig. 12.

Immunolabelling of Cx36 and vglut1 in the MNTB of adult mouse. (A) Low magnification of the same field (A1-A3) showing labelling of vglut1 densely distributed around large neuronal somata (A1, arrows), and Cx36-puncta around neuronal somata counterstained with blue Nissl (A2, arrows), with overlay of green/red images (A3), where most neuronal somata decorated with labelling for vglut1 also display Cx36-puncta (arrows). (B) Higher magnification of the same field (B1-B3), showing the punctate appearance of labelling for Cx36 around large neuronal somata (B1, arrows), the restricted localization of labelling to neuronal somata as seen with blue Nissl counterstaining (B2, arrows), and the distribution of

Cx36-puncta in relation to labelling for vglut1 in overlay (B3, arrows). Cx36-puncta are absent around smaller neuronal cell bodies (B2, arrowhead). (C-D) Confocal images showing Cx36-puncta around a soma periphery (C1, arrows) and, in the same field, co-localization of these puncta with labelling for vglut1 (C2, arrows). Similar images through the top surface of a neuronal soma, with labelling of Cx36 (D1) and vglut1-positive terminals viewed en face, showing association of Cx36-puncta with the terminals (D2, arrows).

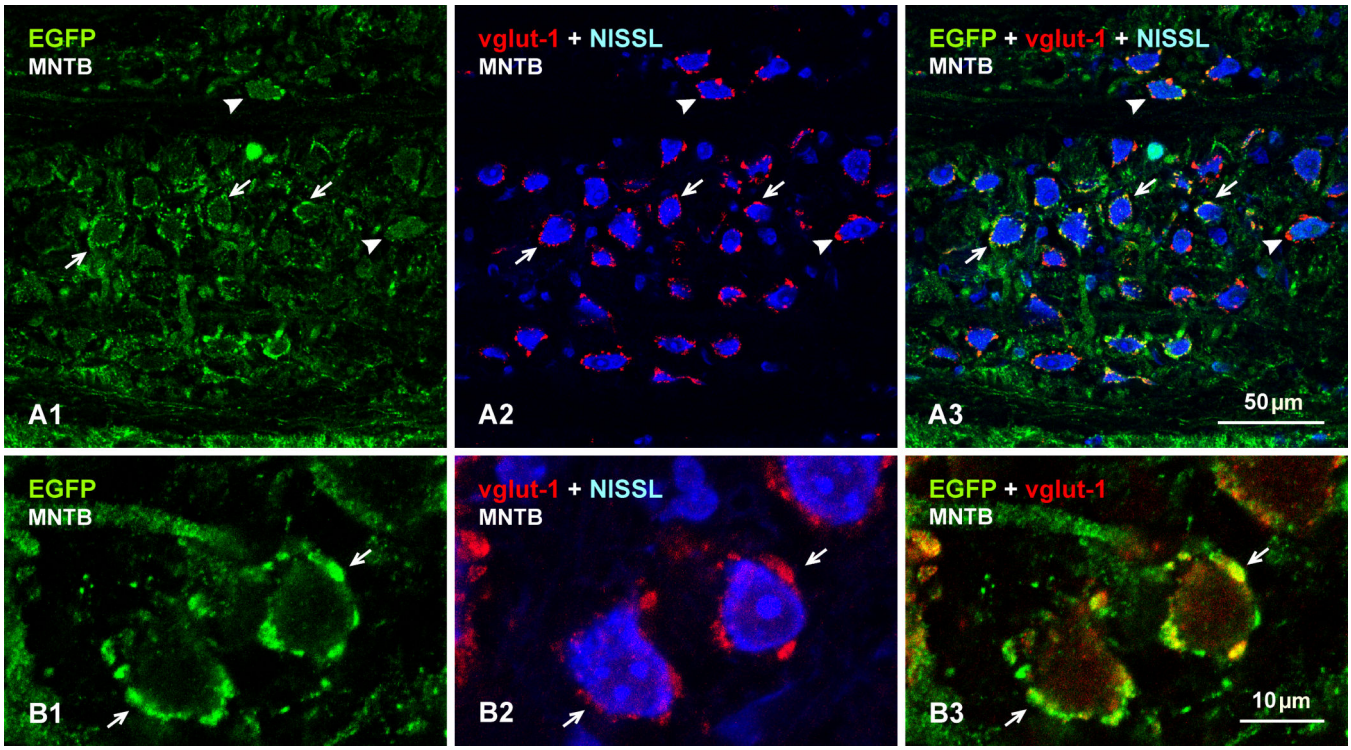

Fig. 13.

Localization of EGFP (green) and vglut1 (red) around neuronal somata in the MNTB of EGFP-Cx36 adult mouse. (A) The same field (A1-A3) showing weak labelling of EGFP in neuronal processes and cytoplasm (A1, arrowheads), and dense labelling of EGFP around the periphery of neuronal somata (D1, arrows) that are contacted by vglut1-positive terminals (A2, arrows), with overlay indicating co-distribution of EGFP and vglut1 around neuronal somata (A3, arrows). (B) Higher magnification confocal images from a similar area as in (A), showing the same field (B1-B3), where labelling for EGFP (B1, arrows) is seen co-localized with labelling of vglut1 (B2, arrows; and B3 in overlay) around MNTB neuronal somata.

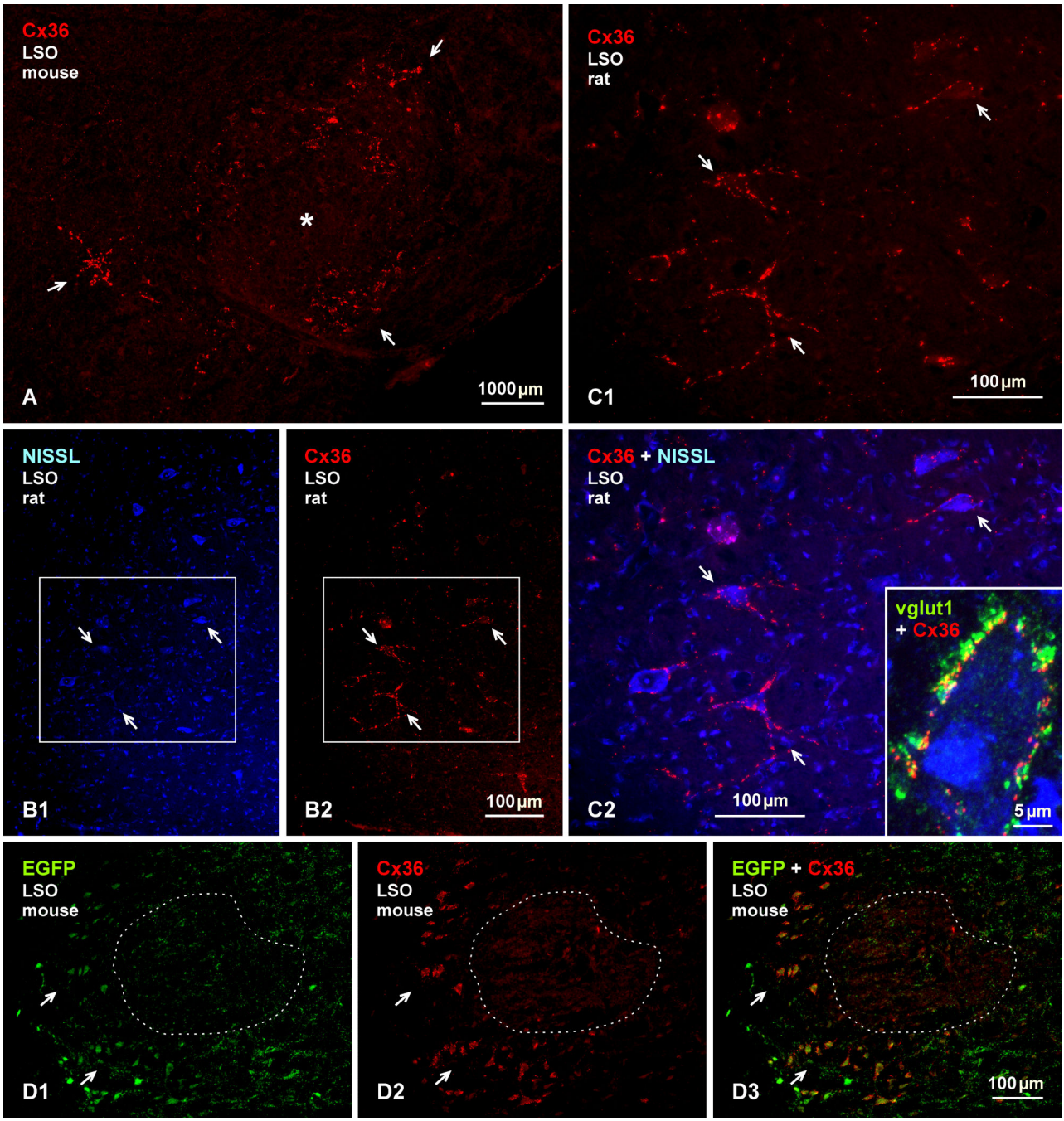

Fig. 14.

Distribution of Cx36 and EGFP around the periphery of the LSO. (A) Immunofluorescence labelling of Cx36 in adult mouse, showing Cx36 localized around the peripheral margins of the LSO (arrows), with the LSO itself largely devoid of labelling (asterisk). (B) Images of the lateral margin of rat LSO, showing large Nissl counterstained neurons in the region (B1, arrows) and labelling of Cx36 along this margin (B2, arrows). (C) Magnification of the boxed areas in (B) with labelling for Cx36 alone (C1) and after overlay with blue Nissl counterstain (C2), showing punctate appearance of labelling for Cx36 and association of

Cx36-puncta with most of the relatively large periolivary neuronal somata (arrows). The inset in C2 shows co-localization of Cx36-puncta with vglut1-positive terminals on neuronal somata in the periolivary region. (D) Immunofluorescence labelling of EGFP and Cx36 at the peripheral margins of the LSO in EGFP-Cx36 mouse, showing weak labelling for EGFP within large neuronal somata along the lateral and ventral LSO margins (D1, arrows) and, in the same field, labelling for Cx36 along these margins (D2, arrows), where Cx36 is localized to EGFP-positive neurons, as shown in overlay (D3, arrows). The LSO itself (outlined by dotted line) shows only background green and red fluorescence.

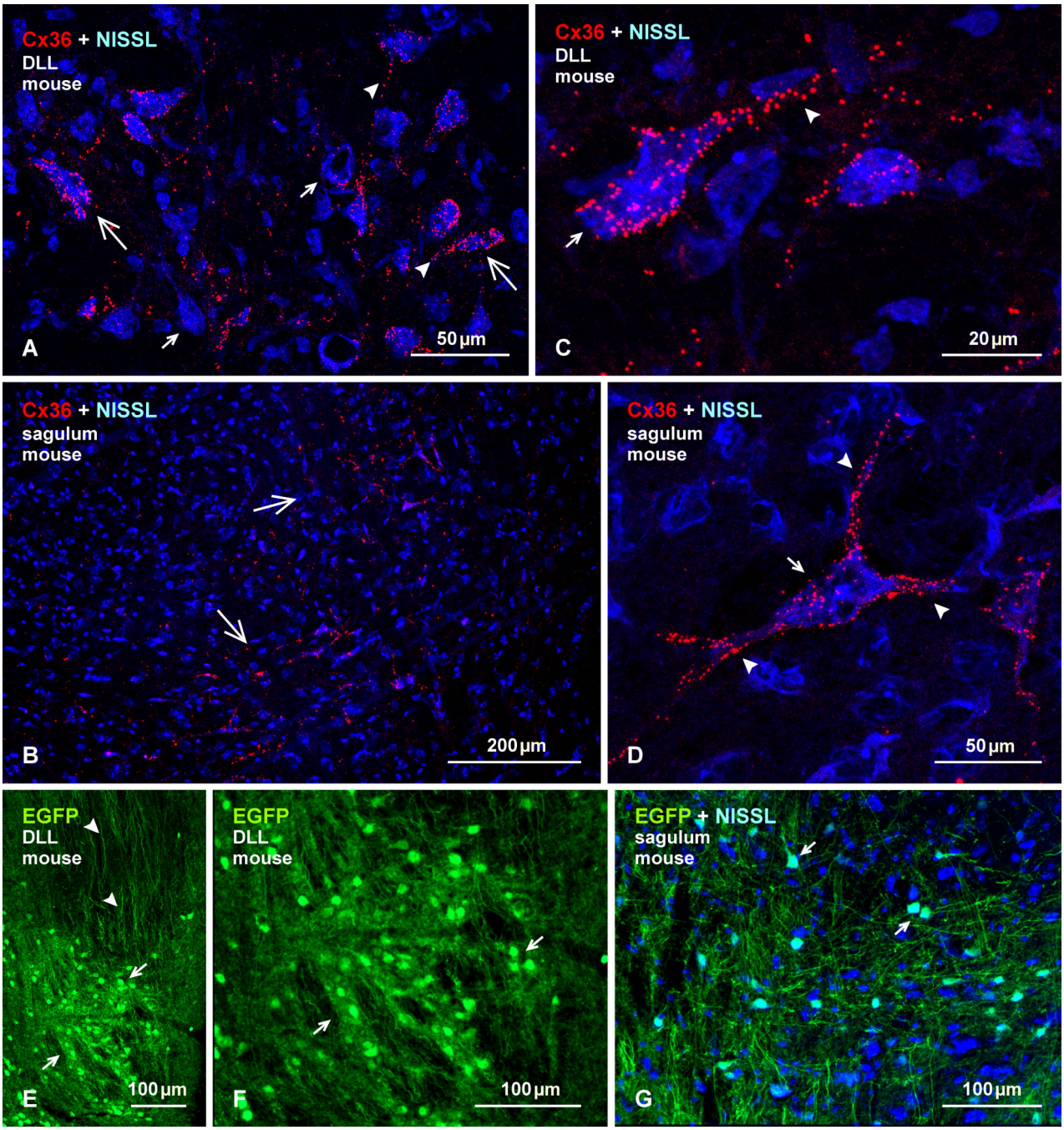

Fig. 15.

Immunofluorescence labelling of Cx36 and EGFP in the DLL and nucleus sagulum of adult mouse. (A, B) Labelling of Cx36 with blue Nissl counterstaining in the DLL (A), showing Cx36-puncta heavily concentrated on some large neuronal somata (large arrows) and their initial dendrites (arrowheads), and sparsely distributed or absent on others (small arrows). In the sagulum (B), Cx36-puncta are moderately distributed on medium sized neurons in the medial and ventromedial portions of the nucleus (arrows). (C, D) Magnification of neurons in the DLL (C) and sagulum (D), showing collections of Cx36-puncta on the surface of

neuronal somata (arrows) and initial dendrites (arrowheads), which was commonly seen in DLL, but only on a few neurons per section had this density of puncta in the sagulum. (E, F) Immunolabelling of EGFP in the DLL in adult EGFP-Cx36 mice viewed at low (E) and higher (F) magnification, showing intense labelling for EGFP in neuronal cell bodies (arrows), and dense collections of dorsally located EGFP-positive axons (arrowheads). (G) The nucleus sagulum with blue Nissl counterstain, showing labelling of EGFP in a subpopulation of neurons (arrows).

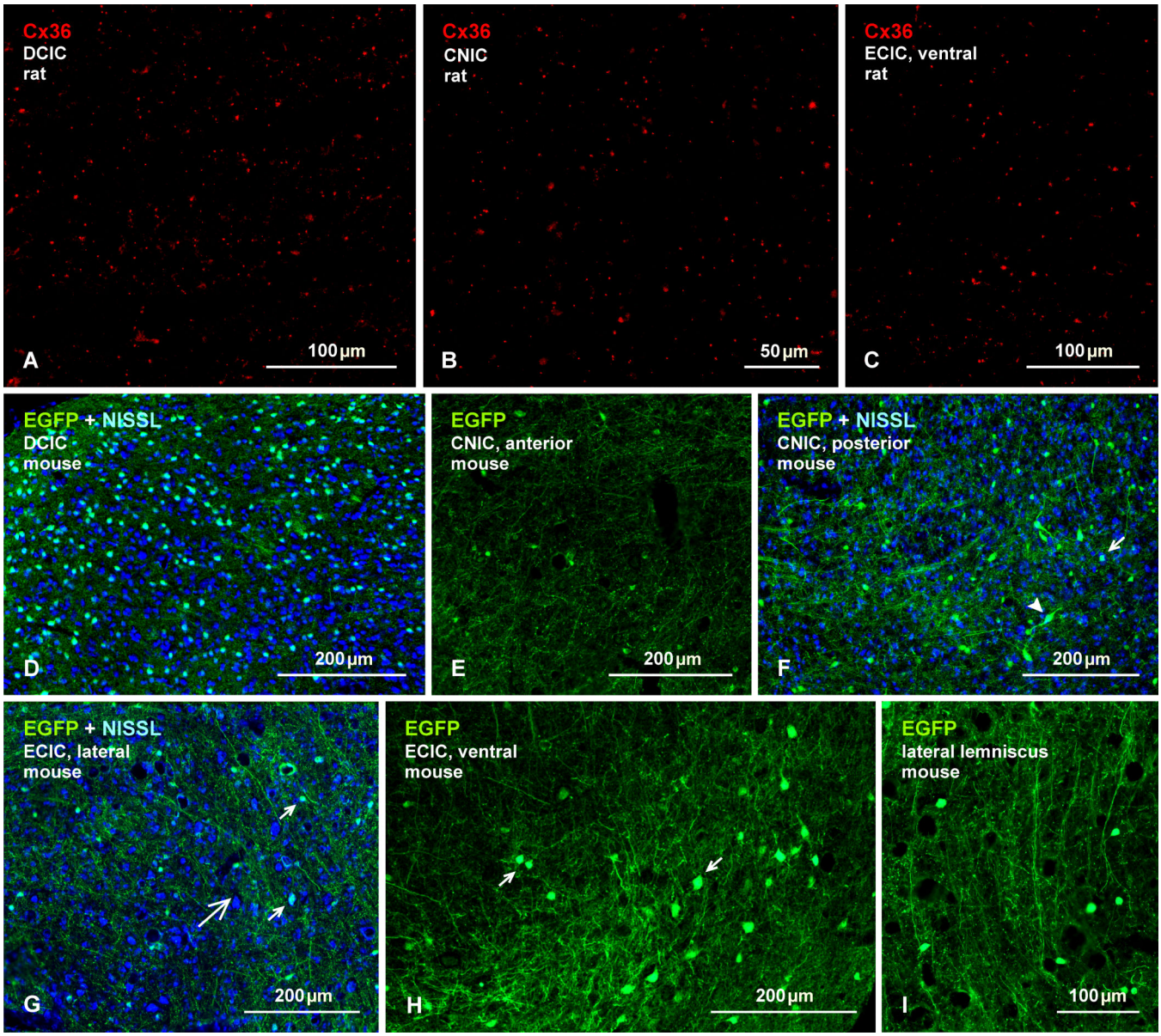

Fig. 16.

Immunofluorescence labelling of Cx36 and EGFP in the IC. (A-C) Adult rat IC, showing sparse to moderate density of Cx36-puncta in each of its major subdivisions. Cx36-puncta range from fine to coarse calibre in the dorsal cortex (A; DCIC), the central nucleus (B; CNIC), and the external cortex (C; ECIC). (D-I) Immunolabelling of EGFP in EGFP-Cx36 mice, showing a heterogeneity in the density of EGFP-immunopositive neurons; the medial portion of the DCIC has the highest density (D) and anterior regions of the CNIC has the lowest density (E). Posterior areas of the CNIC has a moderate density of small (F, arrow) and large (F, arrowhead) neurons. (G-I) The ECIC at a lateral location (G, large arrow), showing EGFP in scattered neurons (G, small arrows) and in neuronal processes, and in a ventrolateral location showing EGFP in a dense collection of neuronal somata (H, arrows). More ventrally, a EGFP-positive axons (I) are seen entering the ventral ECIC.

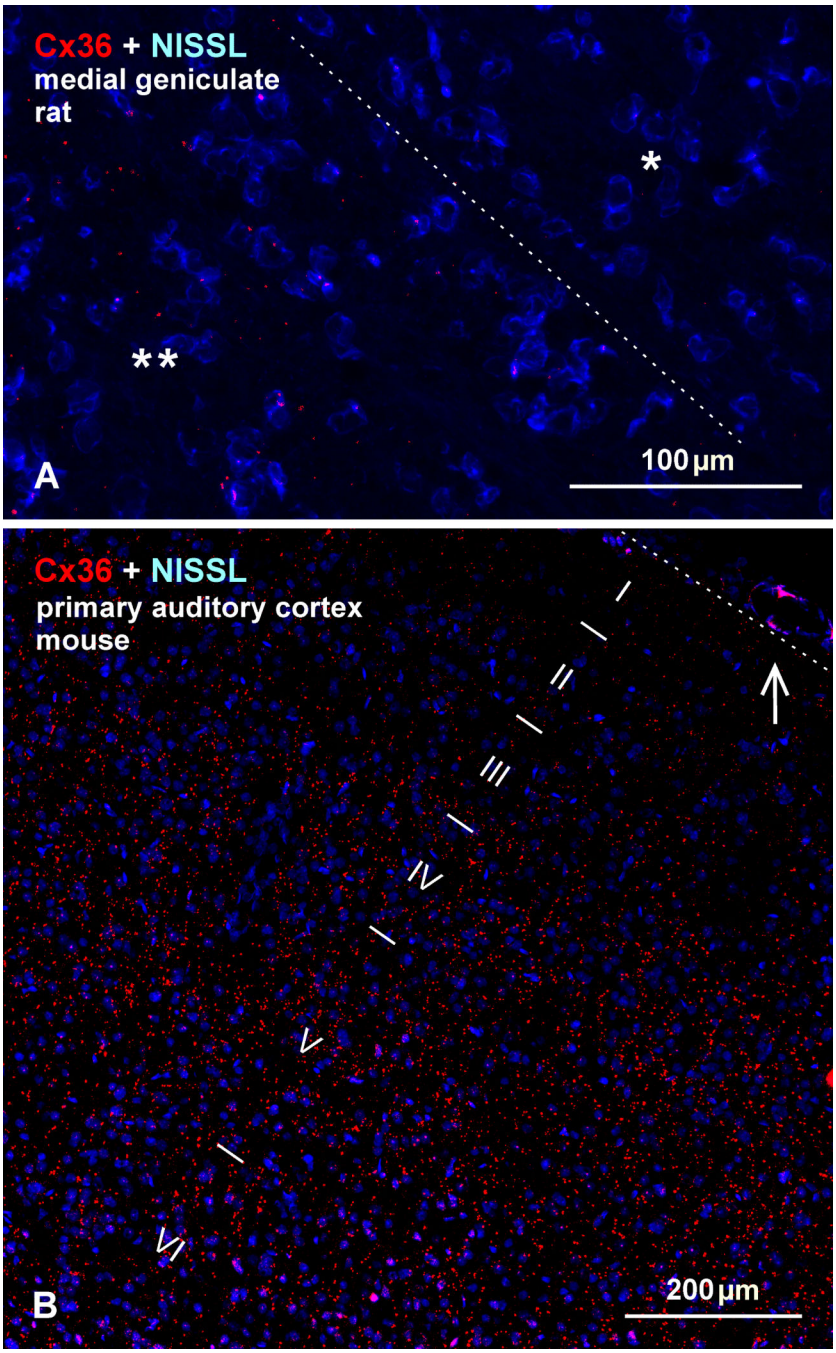

Fig. 17.

Immunofluorescence labelling of Cx36 in the thalamus and primary auditory cortex. (A) Image showing absence of labelling for Cx36 in the medial geniculate nucleus of adult rat, shown in its ventromedial quadrant (asterisk) bordering the posterior thalamic triangular nucleus (double asterisk), in which labelling is shown as positive control for Cx36 detection in a blue Nissl counterstained section (dotted line indicates border between the two nuclei). (B) Labelling of Cx36 in the primary auditory cerebral cortex with blue Nissl counterstaining in adult mouse. Dotted line (upper right) shows auditory cortical surface,

arrow points to dorsal, and numerals indicate cortical layers. Cx36-puncta are barely detectable in layer I, very sparse in layer II, and sparse in layer III. In deeper layers, Cx36-puncta are distributed at moderate density in layer IV and V, and are of slightly lower density in layer VI.